Elastic Property of Returned Samples From Asteroid (162173) Ryugu

Keisuke Onodera[1], Yuta Ino[2,3], Satoshi Tanaka[3], Taichi Kawamura[4], Rei Kanemaru[3], Takuya Ishizaki[3], Ryota Fukai[3], Takeshi Tsuji[1], Tomoki Nakamura[5], Daisuke Nakashima[5], Masayuki Uesugi[6], Shogo Tachibana[1], Seiji Sugita[1], Hisayoshi Yurimoto[7], Takaaki Noguchi[8], Ryuji Okazaki[9], Hikaru Yabuta[10], Hiroshi Naraoka[9], Kanako Sakamoto[3], Toru Yada[3], Masahiro Nishimura[3], Aiko Nakato[3], Akiko Miyazaki[3], Kasumi Yogata[3], Masanao Abe[3], Tatsuaki Okada[3], Tomohiro Usui[3], Makoto Yoshikawa[3], Takanao Saiki[3],Fuyuto Terui[11], Satoru Nakazawa[3], Sei-ichiro Watanabe[12],Yuichi Tsuda[3]

[1]The University of Tokyo, Tokyo, Japan.
[2]Kwansei Gakuin University, Sanda, Japan.
[3]Institute of Space and Astronautical Science, Japan Aerospace Exploration Agency, Sagamihara, Japan.
[4]Institut de Physique du Globe de Paris, Universié Paris Cité, Paris, France.
[5]Tohoku University, Sendai, Japan.
[6]Japan Synchrotron Radiation Research Institute (JASRI), SPring-8, Hyogo, Japan.
[7]Hokkaido University, Sapporo, Japan.
[8]Kyoto University, Kyoto, Japan.
[9]Kyushu University, Fukuoka, Japan.
[10]Hiroshima University, Hiroshima, Japan.
[11]Kanagawa Institute of Technology, Atsugi, Japan.
[12]Nagoya University, Nagoya, Japan.

Key Points:

- We report the initial summary of the elastic property of asteroid (162173) Ryugu samples brought by Hayabusa2.
- The measured elastic parameters were compared with those of carbonaceous chondrites.
- We found that the Ryugu samples show high similarity in elastic properties to the Tagish Lake meteorite.

Corresponding author: Keisuke Onodera, onodera@eri.u-tokyo.ac.jp

Abstract

The elastic property of asteroids is one of the paramount parameters for understanding their physical nature. For example, the rigidity enables us to discuss the asteroid's shape and surface features such as craters and boulders, leading to a better understanding of geomorphological and geological features on small celestial bodies. The sound velocity allows us to construct an equation of state that is the most fundamental step to simulate the formation of small bodies numerically. Moreover, seismic wave velocities and attenuation factors are useful to account for resurfacing caused by impact-induced seismic shaking. The elastic property of asteroids thus plays an important role in elucidating the asteroid's evolution and current geological processes. The Hayabusa2 spacecraft brought back the rock samples from C-type asteroid (162173) Ryugu in December 2020. As a part of the initial analysis of returned samples, we measured the seismic wave velocity of the Ryugu samples using the pulse transmission method. We found that P- and S-wave velocities of the Ryugu samples were about 2.1 km/s and 1.2 km/s, respectively. We also estimated Young's modulus of 6.0 – 8.0 GPa. A comparison of the derived parameters with those of carbonaceous chondrites showed that the Ryugu samples have a similar elastic property to the Tagish Lake meteorite, which may have come from a D-type asteroid. Both Ryugu and Tagish Lake show a high degree of aqueous alteration and few high-temperature components such as chondrules, indicating that they formed in the outer region of the solar system.

Plain Language Summary

The elastic property is one of the paramount parameters to characterize the shape and surface morphology of asteroids. It also provides a key constraint in modeling the formation process of small bodies. Therefore, it is of great importance to measure elastic parameters to understand the current surface geology and the evolution of asteroids. The JAXA's Hayabusa2 spacecraft brought back rock samples from C-type asteroid Ryugu. As a part of the initial analysis of the Ryugu samples, some fundamental physical properties were studied. Here we report the initial summary of the elastic property of the Ryugu samples. We measured the seismic wave velocity of the Ryugu sample and estimated their rigidity such as the Young's modulus. We found that P- and S-wave velocities and Young's modulus were 1.9 – 2.4 km/s, 1.2 – 1.4 km/s, and 6.0 – 8.0 GPa, respectively. Comparing these results with those for carbonaceous chondrites, we confirmed that the elastic property of Ryugu samples showed a high similarity to that of the Tagish Lake meteorite that underwent aqueous alteration and has few chondrules like the Ryugu samples.

1 Introduction

On December 6th, 2020, after six years of space journey, Hayabusa2 brought back samples from C-type asteroid (162173) Ryugu. The samples were collected at two equatorial sites: touch-down site 1 (TD1) and touch-down site 2 (TD2) (e.g., Morota et al., 2020; Tachibana et al., 2022). The TD2 is situated in the vicinity of the artificially formed crater through the impact experiment (Arakawa et al., 2020). The total amount of the collected samples reached 5.4 g with the size ranging up to 10 mm (e.g., Yokoyama et al., 2022; Tachibana et al., 2022). A part of them was allocated to the Hayabusa2 initial analysis team to study the chemical and physical properties of the Ryugu samples (e.g., Yokoyama et al., 2022; T. Nakamura et al., 2022; M. Sato et al., 2022).

The sample analysis from the chemical and mineralogical aspects has shown that Ryugu is similar to CI (Ivuna-type) chondrites, which suffered aqueous alteration but keeps the most primitive materials (e.g., Yada et al., 2022; Yokoyama et al., 2022; Ito et al., 2022; T. Nakamura et al., 2022). This indicates that the Ryugu's parent body formed in the outer solar system (e.g., T. Nakamura et al., 2022).

On the other hand, the measured bulk density ($\sim$ 1,800 kg/m^3; T. Nakamura et al., 2022) shows that Ryugu has more in common with the Tagish Lake meteorites — the most fragile meteorites ever discovered (e.g., Zolensky et al., 2002). This implies that the Ryugu samples are porous and mechanically weak (i.e., low rigidity). Since there are few studies evaluating the mechanical properties of aqueously altered chondrites (e.g., CI, Tagish Lake, Tarda), the comparison in terms of physical properties has not been realized yet. In this study, we report the elastic properties of the Ryugu samples together with the results for the aqueously altered chondrites so that we can add the description of the returned samples from a different aspect.

The elastic property (e.g., Young's modulus, elastic wave velocity, and density) is one of the fundamental parameters to characterize a solid celestial body. It should help us better constrain the Ryugu's formation scenario as well as improve our knowledge of the phenomena occurring under the microgravity condition such as the resurfacing effect (e.g., Richardson et al., 2004; Honda et al., 2021; Takaki et al., 2022). Especially, the sound velocity and the Grüneisen parameter are key factors in building the equation of state, which is essential for the numerical simulation of catastrophic impact — a key process to form rubble-pile bodies. Using the initial estimates of Ryugu's elastic properties, T. Nakamura et al. (2022) performed numerical calculations to simulate the thermal evolution and catastrophic destruction of Ryugu's parent body.

The physical properties of the returned samples also allow us to solve the discrepancy between theoretical prediction and actual observation of the artificial impact event. Nishiyama et al. (2021) simulated the seismic signals excited by the artificial impact — Small Carry-on Impactor (SCI) impact (Saiki et al., 2013; Arakawa et al., 2020). It was expected that resurfacing could occur due to seismic shaking considering the kinetic energy provided by the SCI impact. Some surface rocks and boulders moved due to the impact, however, the lateral displacement was smaller than expected (Honda et al., 2021; Nishiyama et al., 2021). This discrepancy between the theory and observations has not been solved yet, and investigation of seismic wave propagation under microgravity conditions is called for. Since the resurfacing effect is one of the fundamental processes in the surface evolution of solid celestial bodies, it is of great importance to grasp the elastic behavior on the asteroid's surface through the measurements of the returned samples.

In this study, we evaluated the elastic property of the Ryugu samples such as elastic wave velocity and rigidity together with the inelastic attenuation factor, which were obtained for the first time from the returned asteroid samples. Our results are expected (i) to fill in the gap between theory and the observations with regard to the elastic behavior on the asteroid and (ii) to reconstruct the Ryugu's bulk elastic property, both of which are pivotal to constructing a more precise model of the surface evolution of the asteroid.

Some of the results have been reported by T. Nakamura et al. (2022), but here we present the refined results with some additional measurements that were not included in their report. Moreover, we compare the parameters obtained from the Ryugu samples with those of other carbonaceous chondrites to discuss whether the Ryugu samples are similar to or different from any carbonaceous chondrites.

In the following sections, we describe the measured samples and the experimental settings for the pulse transmission method. Then, we show the elastic property of the Ryugu samples, followed by discussions on the comparison with carbonaceous chondrites.

2 Method

2.1 Samples used for measurements

Our team — a part of "Team Stone" in the Hayabusa2 initial analysis team — measured the elastic wave velocity of C0002-No3 and C0002-No4. These samples were cut out from one of the largest fragments in the samples collected at TD2. As shown in Figures 1a-b, each sample was a few mm wide and long with thicknesses of 0.7 – 1 mm (the first to the third rows in Table 1). The details of the sample preparation — such as fixing the samples with glycol phthalate, making plates by slicing with a diamond saw, polishing the sample surfaces, and removing glycol phthalate — were done by Nakashima et al. (2022) and T. Nakamura et al. (2022). Because C0002-No4 was split into two pieces (No4-1 and No4-2; Figure 1b) over the successive measurements of physical properties (T. Nakamura et al., 2022), we regarded these pieces as different samples and measured the seismic wave velocity individually.

In addition to the Ryugu samples, we also measured several carbonaceous chondrites for comparison (the fourth to tenth rows in Table 1). The elastic property of Tagish Lake (C2) and Ivuna (CI) had never been measured before (e.g., Ostrowski & Bryson, 2019), so this report describes their elastic property for the first time.

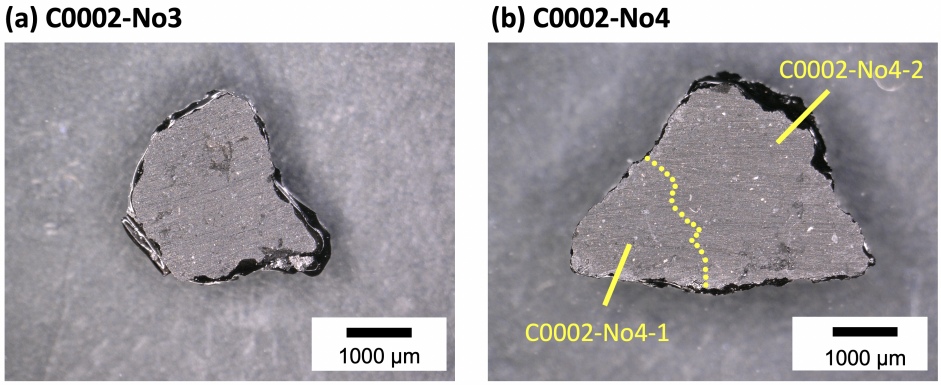

Figure 1. Optical images of the Ryugu samples with polished surfaces: (a)C0002-No3 and (b)C0002-No4 that was split into two fragments (C0002-No4-1 and No4-2) over the successive geophysical measurements (T. Nakamura et al., 2022).

2.2 The principle of measurements and experimental settings

We employed the pulse transmission method, which is a common method to measure the elastic wave velocity (e.g., Birch, 1960). The principle is to measure the travel time t_d of a pulse passing through a medium with a thickness of d. Dividing d with t_d gives us a seismic wave velocity. Figure 2a illustrates a schematic diagram of the experimental setting where a sample is put between transducers; one of which is connected with a pulsar and the other is connected with an oscilloscope via an amplifier. The instruments used for the measurements are summarized in Figure 2b.

We developed a new measurement system for a small sample (sub-micron to 1 mm scale) under a less loaded condition (< 10 MPa) because the sample was expected to be fragile and porous (e.g., Sugita et al., 2019; Grott et al., 2019; Arakawa et al., 2020). The developed system is shown in Figure 2c. The 20 MHz and 10 MHz transducers made by OLYMPUS corporation were used (Figure 2b). Under the condition of room temperature and atmospheric pressure, the measurements were conducted as shown in Figure

Table 1. The measured samples and their dimensions.

Sample name	Group	Thickness (mm)	Mean surface area (mm^2)	Bulk density (kg/m^3)
C0002-No3		0.788 ± 0.005	5.74 ± 0.41	
C0002-No4-1		0.943 ± 0.005	2.52 ± 0.86	1823 ± 50
C0002-No4-2		0.950 ± 0.005	6.45 ± 0.82	(T. Nakamura et al., 2022)
Tarda-No0	C2	0.634 ± 0.010	4.53 ±0.33	2220 ± 117
Tarda-No1	C2	0.930 ± 0.006	9.39 ±2.25	2233 ± 106
Tarda-No3	C2	0.961 ± 0.007	3.54 ±2.32	2363 ± 113
Tagish Lake	C2	0.745 ± 0.010	7.03 ± 0.88	1768 ± 89
Murchison	CM	0.650 ± 0.005	7.94 ± 0.12	2522 ± 126
Ivuna	CI	1.306 ± 0.007	4.85 ± 1.43	2444 ± 116

158 2d where the loading was controlled manually. In this study, we mainly show the results
159 obtained under ∼ 1 MPa loading.

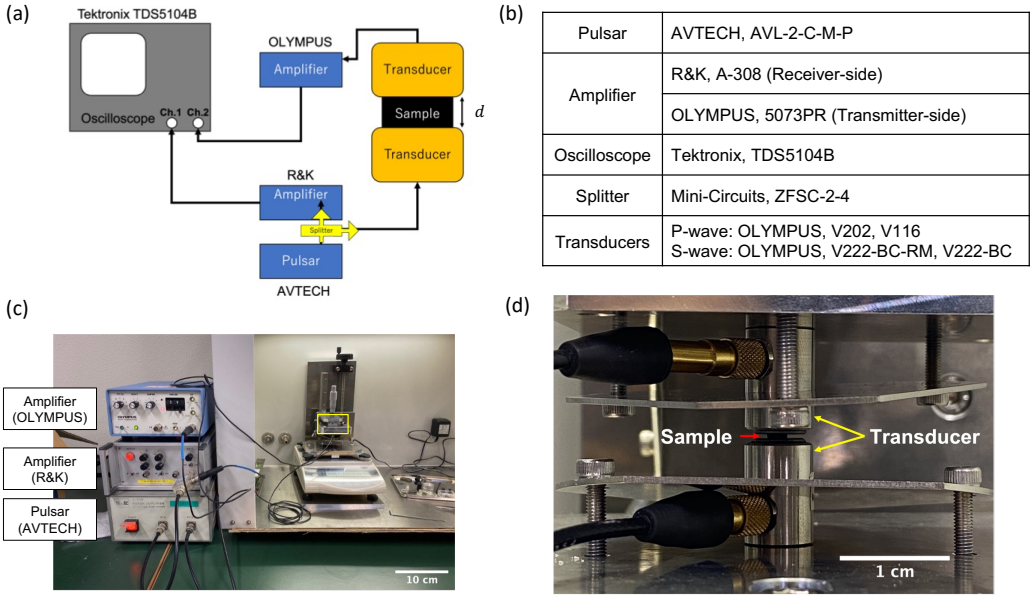

Figure 2. (a)Schematic diagram of the experimental setting. (b) The instruments used in this study. (c)The actual measurement setting. (d)Close-up of the yellow box in (c). The sample is sandwiched with two transducers.

160 ### 2.3 Evaluation of elastic parameters

161 Three types of signals were collected for each sample. The first signal is the back-
162 ground signal S_{bg}, which is the signal excited by the experimental system itself when trans-
163 ducers are uncontacted. The second one is the signal without sample S_{ns}, which is mea-

sured by contacting two transducers. The third is the signal with sample S_{sp} measured with a sample sandwiched between the transducers.

Each type of signal was measured multiple times to stack the signals and to evaluate random errors in the measurement. We then obtained the stacked and averaged background signal $\overline{S_{bg}}$ to enhance the long-period background components for properly removing them from S_{sp} and S_{ns}. The removed signals are defined as follows:

$$\begin{aligned} S_{sb}(t) &= S_{sp}(t) - \overline{S_{bg}}(t), \\ S_{nb}(t) &= S_{ns}(t) - \overline{S_{bg}}(t), \end{aligned} \tag{1}$$

where t is time. Figures 3a-c shows an example of the signals obtained in this study.

We applied band-pass filtering between 2 MHz and 15 MHz when reading the time delay in order to suppress the noises and enhance the input pulse. Measuring the time delay of the peak signal of S_{sb} from that of S_{nb} gives us the lag-time t_d — a travel time through a sample. We performed the measurements five times (Figure 3d), and the average lag-time $\overline{t_d}$ and the standard deviation Δt_d were used to determine the elastic wave velocity v and its error Δv as shown below:

$$\begin{aligned} v &= \tfrac{d}{\overline{t_d}}, \\ \Delta v &= \sqrt{\left(\tfrac{\Delta d}{\overline{t_d}}\right)^2 + \left(\tfrac{d}{\overline{t_d}^2}\Delta t_d\right)^2}. \end{aligned} \tag{2}$$

With P- and S-wave velocities (v_p and v_s), the Poisson's ratio can be written as follows:

$$\nu = \frac{v_p^2 - 2v_s^2}{2(v_p^2 - v_s^2)}. \tag{3}$$

Combining v_p and v_s with the sample density (ρ), we can evaluate Young's modulus (E), the bulk modulus (K), and the shear modulus (μ) as follows:

$$\begin{aligned} E &= \tfrac{3v_p^2 - 4v_s^2}{v_p^2 - v_s^2}\rho v_s^2, \\ K &= \rho\left(v_p^2 - \tfrac{4}{3}v_s^2\right), \\ \mu &= \rho v_s^2. \end{aligned} \tag{4}$$

2.4 Evaluation of inelastic attenuation: Quality factor

With the spectral fitting method commonly used in seismology, we evaluated the attenuation factor Q — the rate of the energy loss due to the absorption by a medium and scattering effects coming from the heterogeneity within a sample. Considering both geometrical spreading and absorption effects, the spectra of S_{nb} and S_{sb} are expressed as:

$$\begin{aligned} S_{nb}(f) &\propto \tfrac{1}{d_{tr}^2} e^{-\frac{2\pi d_{tr}}{v_{tr}Q_{tr}}f}, \\ S_{sb}(f) &\propto \tfrac{1}{(d_{tr}+d)^2} e^{-\frac{2\pi d_{tr}}{v_{tr}Q_{tr}}f} e^{-\frac{2\pi d}{vQ}f}, \end{aligned} \tag{5}$$

where d_{tr}, v_{tr}, and Q_{tr} are the height of the contacted transducers, the elastic wave velocity of the transducers, and the attenuation factor of the transducers. Dividing $S_{sb}(f)$ with $S_{nb}(f)$ gives us

$$S_{fit}(f) = \frac{S_{sb}(f)}{S_{nb}(f)} \propto e^{-\frac{2\pi d}{vQ}f}. \tag{6}$$

Figure 4a shows the amplitude spectral densities for S_{nb} (black) and S_{sb} (red) and Figure 4b displays the decomposed spectra corresponding to $S_{fit}(f)$. The frequency band of 2 MHz – 10 MHz was used for the fitting. The fitted curve (thick broken line) and the error range (dotted lines) are presented in Figure 4b.

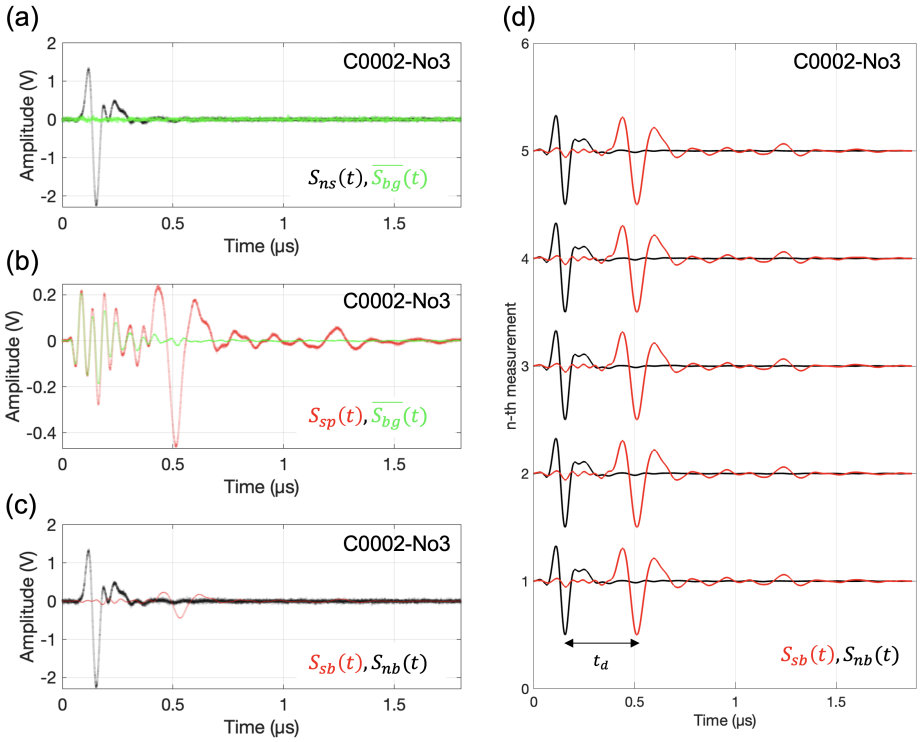

Figure 3. Typical examples of the measured signals for P-wave. (a) The stacked signal of the background $\overline{S_{bg}}$ (green) and the signal without sample S_{ns} (black). (b) $\overline{S_{bg}}$ (green) and the signal with sample S_{sp} (red). (c) The signals with $\overline{S_{bg}}$ removed from S_{ns} (i.e., S_{nb} in black) and S_{sp} (i.e., S_{sb} in red). (d) All the S_{nb} and S_{sb} signals obtained in the five repeated measurements for C0002-No3. The respective signals are band-pass filtered between 2 MHz - 15 MHz to enhance the incident pulse. Note that the signals are arbitrarily shifted.

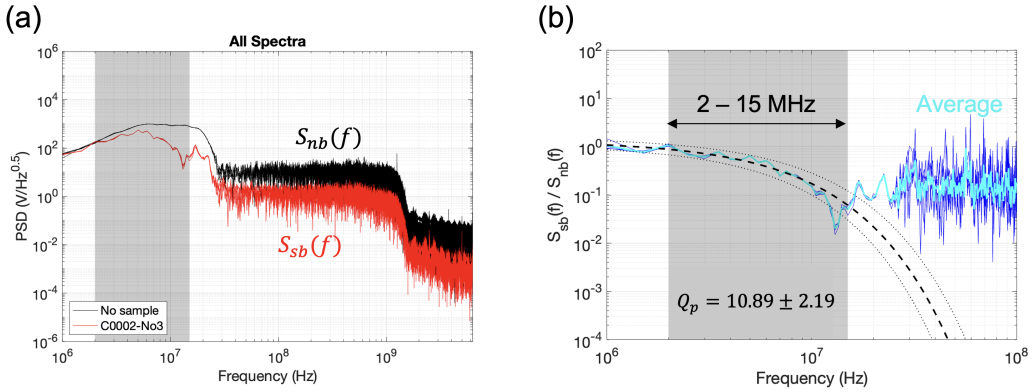

Figure 4. (a) Amplitude spectral densities (ASDs) for S_{nb} (black) and S_{sb} (red). The grey shaded area shows the frequency band used for fitting. (b) The deconvolved spectra (S_{sb}/S_{nb}). The individual spectrum and the averaged spectrum are shown in blue and cyan, respectively. The thick broken line represents the best-fitted curve and the dotted lines display the error range.

3 Results and Discussion

3.1 Seismic wave velocity and Young's modulus

The obtained seismic wave velocity and Young's modulus for C0002-No3, C0002-No4-1, and C0002-No4-2 are shown in the first three rows in Table 2. For P- and S-wave velocities, we obtained V_p = 1.9 – 2.2 km/s and V_s = 1.1 – 1.3 km/s, respectively. Combining the V_p and V_s with the bulk density in Table 1 leads to Young's modulus of 6.0 – 7.5 GPa (the first three rows in Table 3). Table 2 also includes V_p, V_s, and Young's modulus measured for carbonaceous chondrites (Tarda, Tagish Lake, Murchison, and Ivuna).

Table 2. List of measurement results. $P_i (i = p, s)$ is loading pressure in MPa, $V_i (i = p, s)$ is the elastic wave velocity in km/s, and ν is the Poisson's ratio.

Sample name	P_p (MPa)	V_p (km/s)	P_s (MPa)	V_s (km/s)	ν
C0002-No3	0.97 ± 0.43	2.21 ± 0.01	0.69 ± 0.31	1.26 ± 0.01	0.26 ± 0.01
C0002-No4-1	1.06 ± 0.55	1.95 ± 0.01	0.91 ± 0.48	1.20 ± 0.01	0.19 ± 0.01
C0002-No4-2	0.98 ± 0.38	1.94 ± 0.01	0.61 ± 0.25	1.17 ± 0.01	0.22 ± 0.01
C0002-No3-1	5.64 ± 1.79	2.12 ± 0.01	4.31 ± 1.63	1.37 ± 0.01	0.14 ± 0.01
C0002-No3-2	4.50 ± 1.85	2.40 ± 0.02	6.10 ± 2.50	1.25 ± 0.01	0.31 ± 0.01
Tarda-No0	0.90 ± 0.68	2.68 ± 0.04	0.90 ± 0.68	1.52 ± 0.03	0.26 ± 0.02
Tarda-No1	0.99 ± 0.24	2.32 ± 0.02	0.99 ± 0.24	1.47 ± 0.01	0.16 ± 0.02
Tarda-No3-1	1.00 ± 0.66	2.47 ± 0.02	1.25 ± 0.82	1.55 ± 0.02	0.18 ± 0.02
Tagish Lake	1.39 ± 0.38	1.86 ± 0.03	1.39 ± 0.38	1.13 ± 0.02	0.21 ± 0.02
Murchison	0.87 ± 0.46	3.77 ± 0.03	0.87 ± 0.46	1.97 ± 0.02	0.31 ± 0.01
Ivuna	1.01 ± 0.30	2.38 ± 0.01	1.01 ± 0.30	1.63 ± 0.01	0.06 ± 0.02

3.2 Variation of the elastic property within a mm-sized sample

We performed an additional measurement for C0002-No3 after the bending experiment (T. Nakamura et al., 2022) over which the sample was destroyed into fragments. We used two pieces out of the split fragments (Figures 5a-b; C0002-No3-1 and C0002-No3-2) to investigate a variation in elastic property within a sample. Although there was little difference in elastic property between C0002-No4-1 and C0002-No4-2, we found a 10% difference in the seismic wave velocity between C0002-No3-1 and No3-2 (the fourth and fifth rows in Table 2).

To explain the 10% variation of the seismic wave velocity, we looked into the X-ray computed tomography (X-ray CT) image data (Figures 6a-b), which were obtained at SPring-8, Japan (T. Nakamura et al., 2022). Within the respective CT images for C0002-No3 and C0002-No4, we cut out the 0.68 mm × 0.68 mm areas and made histograms of voxel values, where the larger value corresponds to the denser materials. Figures 6a-b show examples for a certain slice of each sample. Figure 7 gives an example of the voxel values for constituent materials. Keep in mind that it is difficult to determine each constituent mineral because the X-ray CT image only represents the relative density variations that are relevant to the X-ray absorption. Based on the visual features and previous image analyses (e.g., T. Nakamura et al., 2022; Yokoyama et al., 2022), only cracks and phyllosilicate matrices were labeled, while other representative minerals were named

Table 3. List of the estimated elastic parameters such as Young's modulus, the bulk modulus, and the shear modulus. Because we could not measure the bulk density of C0002-No3-1 and C0002-No3-2 individually, the corresponding Young's modulus values were estimated using the values listed in Table 1.

Sample name	Young's modulus (GPa)	Bulk modulus (GPa)	Shear modulus (GPa)
C0002-No3	7.3 ± 0.3	5.05 ± 0.19	2.91 ± 0.09
C0002-No4-1	6.3 ± 0.3	3.40 ± 0.15	2.63 ± 0.09
C0002-No4-2	6.0 ± 0.2	3.54 ± 0.13	2.48 ± 0.07
C0002-No3-1	7.8 ± 0.3	3.63 ± 0.16	3.42 ± 0.10
C0002-No3-2	7.5 ± 0.2	6.71 ± 0.24	2.85 ± 0.09
Tarda-No0	12.9 ± 1.0	9.13 ± 0.74	5.12 ± 0.33
Tarda-No1	11.2 ± 0.1	5.59 ± 0.30	4.83 ± 0.07
Tarda-No3-1	13.3 ± 0.1	6.85 ± 0.43	5.68 ± 0.15
Tagish Lake	5.5 ± 0.4	3.14 ± 0.24	2.25 ± 0.13
Murchison	25.7 ± 1.4	22.79 ± 1.29	9.79 ± 0.51
Ivuna	13.8 ± 0.1	5.23 ± 0.26	6.49 ± 0.08

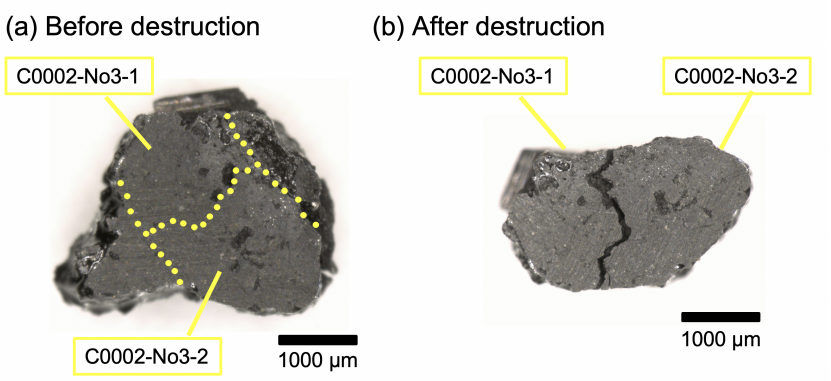

Figure 5. Optical images of C0002-No3 taken (a) before the destruction and (b) after the destruction. The sample was split into four pieces along yellow dotted lines, and the particles named C0002-No3-1 and C0002-No3-2 were used for the measurements.

Mineral 1 and Mineral 2 here. As in Figure 7, Mineral 1 corresponds to the white and small particles, which are the densest materials in the sample (voxel value > 20000). Mineral 2 has the voxel values around 7000 – 15000, ranging sub-millimeters. It is not as dense as Mineral 1, yet denser than the surrounding matrices.

In order to obtain the volumetric information about the relative density distribution within each sample, we made the cumulative histograms over the slice 420–650 (the number corresponds to the identification number of X-ray CT data) for C0002-No3 and the slice 745–1025 for C0002-No4 (Top panels in Figure 8a-b). We quantified the variation of relative density (Bottom panels in Figure 8a-b) from the ratio between the histograms of two different regions. There are some variations in the distribution of cracks, matrices (pixel value < 7000), and Mineral 1 (pixel value > 20000) between two regions in both C0002-No3 and C0002-No4. Considering that C0002-No4-1 and C0002-No4-2 showed almost the same seismic velocity (Table 2), cracks, matrices, and Mineral 1 do

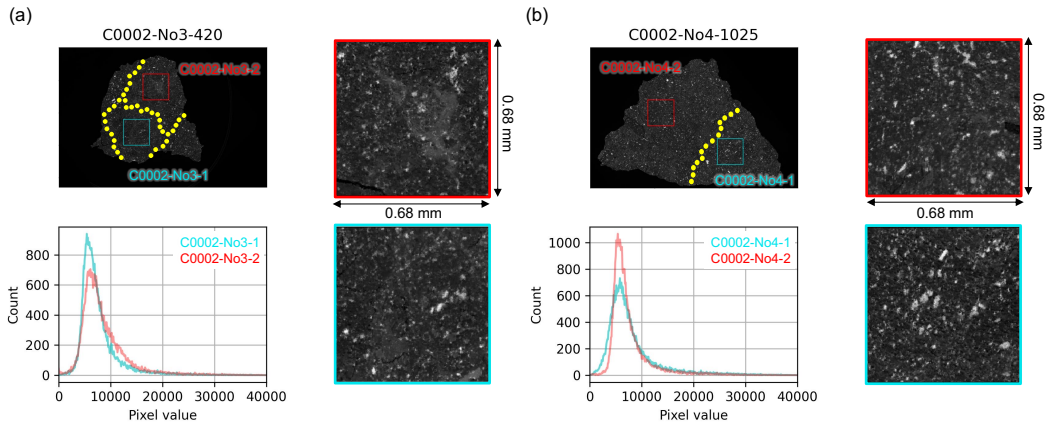

Figure 6. X-ray computed tomography(CT) image for (a) C0002-No3 (Slice 420) and (b) C0002-No4 (Slice 1025) with the voxel resolution of 3.4 μm. In each figure, the left top panel shows the X-ray CT image with the split area divided with yellow dots. The right column displays the expanded images for the trimmed regions (red and cyan areas). The left bottom panel shows the histogram of the voxel value for the respective trimmed areas, where the large voxel values correspond to the brighter (or denser) areas.

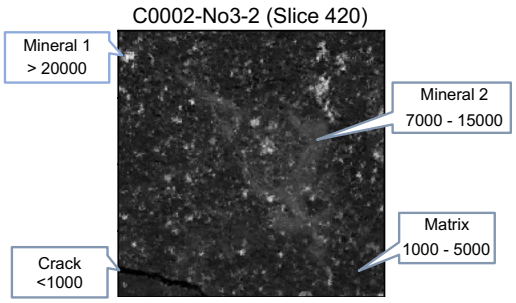

Figure 7. Representative voxel values in the X-ray CT image (Slice 420 of C0002-No3-2).

not have a significant effect on the seismic wave velocity. Focusing on the ratio of Mineral 2, C0002-No3-2 contains more Mineral 2 than C0002-No3-1 by about a factor of 1.5, while there is little difference in the abundance of Mineral 2 between C0002-No4-1 and C0002-No4-2. This indicates that Mineral 2, especially the sub-mm-scale particle of Mineral 2 seen in Figure 7, plays a main role in producing the velocity variation within the C0002-No3 sample. Mineral 2 with the higher voxel values than the surrounding matrix should lead to a 10% larger P-wave velocity of C0002-No3-2 than C0002-No3-1. On the other hand, the S-wave velocity of C0002-No3-2 is smaller than that of C0002-No3-1, which is most likely because C0002-No3-2 contains at least ten times more cracks than C0002-No3-1 (S-wave is more sensitive to porosity or structural heterogeneity within the medium). Further investigation including numerical simulations is needed for more quantitative discussion.

3.3 Inelastic attenuation factor

Inelastic attenuation controls how far the seismic energy can propagate and is thus important to understand the impact-related surface geological processes of asteroids (e.g., resurfacing due to seismic shaking).

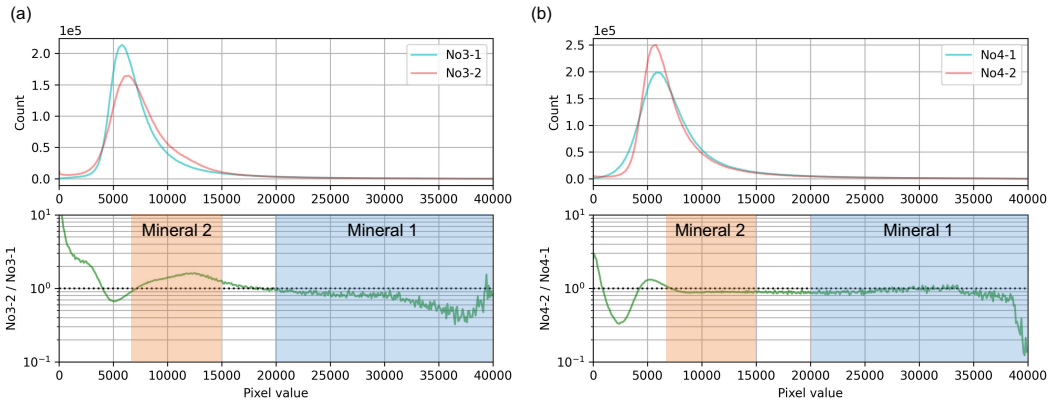

Figure 8. Histograms of voxel values of X-ray CT images and their ratio between different regions of (a) C0002-No3 and (b) C0002-No4. In each panel, the histograms for red and cyan regions in Figures 6a-b are shown at the top, and the histogram ratios are displayed at the bottom.

The spectral fitting approach described in Section 2.4 gives the quality factor Q of 10 – 20 for the Ryugu samples (Table 4). This value is smaller than those of carbonaceous chondrites (20 – 50 in Table 4) and terrestrial rocks (50 – 250) (Kanamori et al., 1970).

Table 4. List of the estimated quality factors. The Q values obtained from P-wave results are presented here because the spectral quality of S-wave was not good enough to determine Q. The Q values for Tarda-No0 and Tarda-No3-1 were not obtained for P-waves either due to the poor spectral quality.

Sample name	Q (P-wave)
C0002-No3	10.9 ± 2.2
C0002-No4-1	9.5 ± 1.7
C0002-No4-2	15.3 ± 4.5
C0002-No3-1	9.5 ± 1.7
C0002-No3-2	13.3 ± 3.0
Tarda-No0	–
Tarda-No1	18.0 ± 5.63
Tarda-No3-1	–
Tagish Lake	36.77 ± 14.49
Murchison	50.86 ± 29.22
Ivuna	16.99 ± 3.85

We here note that the Q values obtained in this study may not be directly applicable to that on the Ryugu's surface although the relative differences between the Ryugu samples and other samples can be discussed. The low Q value was derived for the Apollo returned samples ($Q = 10-30$) (Kanamori et al., 1971; Wang et al., 1971), which was inconsistent with the results of the seismic measurements on the lunar surface ($Q = 3000-7000$) (e.g., Y. Nakamura & Koyama, 1982; Blanchette-Guertin et al., 2012; Onodera et

al., 2022, 2023). The discrepancy between the laboratory measurements and the in-situ seismic experiment was explained by Tittman et al. (1972) and their following works. They conducted Q-value measurements under various environments and assessed how atmospheric conditions and temperature affect the results. They found that the Q value is much more sensitive to humidity, air pressure, and temperature than the elastic wave velocity. For example, when the sample was exposed to hot water for 30 sec, the Q value decreased by 90% compared to the non-exposed condition. They also found that the Q value gets closer to that obtained through seismic observation on the Moon by reducing the air pressure and temperature (e.g., $Q = 800$ under 6.7 $\times 10^{-6}$ Pa at -180°C). In the following experiments (e.g., Tittman et al., 1975, 1976; Tittman, 1977), the Q values as high as those obtained through in-situ lunar seismic observations were achieved after thorough outgassing from the samples under vacuum conditions.

The present results of Q values obtained at 1 atm and the room temperature must thus be affected by these environmental factors. In addition, as attenuation mechanisms could change depending on the frequency range, that needs to be considered when discussing the differences between various frequencies (e.g., Aki & Richards, 1980). For our current measurement, due to some restrictions regarding the available facilities, we could not perform the Q measurements under preferable conditions. However, if we measured the Q-value under ideal conditions, we could effectively evaluate the disparities in Q-value among various samples and different frequency ranges, which would improve our knowledge of the anelastic attenuation on extraterrestrial bodies. In future studies, we plan to measure the Ryugu's Q value under more appropriate conditions.

3.4 Comparison with carbonaceous chondrites

Figures 9a-c are the scatter plots of V_p, V_s, and Young's modulus against the bulk density, comparing our results with the previous measurements of CM (Mighei-type), CO (Ornans-type), and CV (Vigarano-type) chondrites (Jones, 2009; Ibrahim, 2012; Cotto-Figueroa et al., 2016). The aqueously altered carbonaceous chondrites (CI, Tagish Lake, Tarda, and CM) and the Ryugu sample have smaller bulk densities than CO and CV chondrites. Ryugu's V_p, V_s, and Young's modulus range 1.9 – 2.4 km/s, 1.2 – 1.4 km/s, and 6.0 – 8.0 GPa, respectively, and Tagish Lake shows the most similar properties to those of Ryugu samples. The chemical analyses in previous works (e.g., T. Nakamura et al., 2022) indicate that CI chondrites show the highest similarity to the Ryugu samples. On the other hand, the optical feature (e.g., very low-reflectance: 0.02) and the bulk density ($\sim$1,800 kg/m^3) of the Ryugu samples resemble the Tagish Lake meteorites (Zolensky et al., 2002; Yada et al., 2022; T. Nakamura et al., 2022). Through this study, we added a novel description of the Ryugu samples from the aspect of the elastic property. Our results show that the elastic (or mechanical) property of the returned samples is more in accordance with that of Tagish Lake than any other carbonaceous chondrites.

Both Ryugu and Tagish Lake underwent aqueous alteration and have fewer high-temperature inclusions (such as chondrules and CAIs; Zolensky et al., 2002), implying that they formed and evolved under a similar environment. This supports the idea that Ryugu's parent body formed in the outer region of the solar system (e.g, T. Nakamura et al., 2022). Considering the similarities and differences between Ryugu, Ivuna, and Tagish Lake in chemical and physical characteristics, all their parent bodies formed in the outer solar system; but differences in the accumulation process or accumulation region might have produced the variation in chemical and physical properties seen between the three. It is not clear how the evolution processes differ from each other. Yet, further investigation on this topic would give us a better illustration of the early evolution in the outer solar system.

The data for CM, CO, and CV chondrites (Figures 9a-c) are widely scattered, some of which are consistent with the Ryugu samples. To explain the scattered distribution,

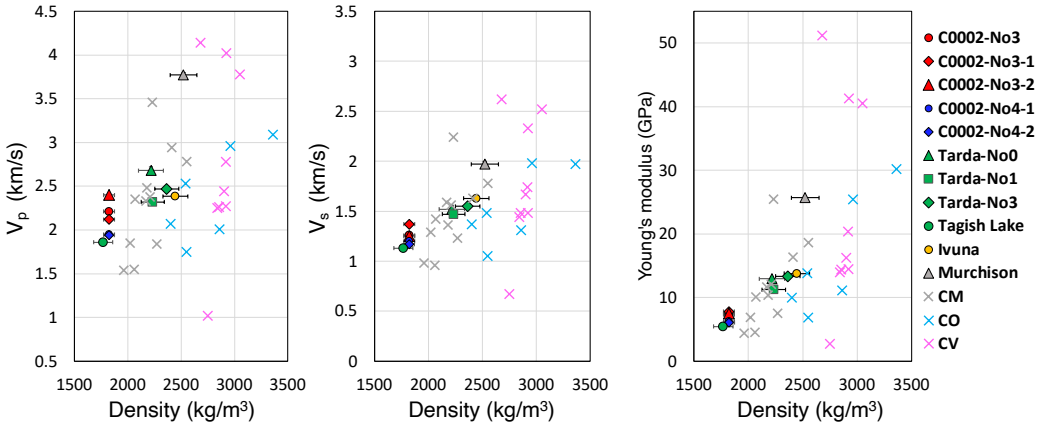

Figure 9. Comparison of the elastic properties of Ryugu and carbonaceous chondrites in this work (closed symbols) with previously reported values for CM, CV, and CO chondrites (colored crosses; Jones, 2009; Ibrahim, 2012; Cotto-Figueroa et al., 2016). (a) P-wave velocity, (b) S-wave velocity, and (c) Young's modulus.

we looked into the relationship between the elastic properties and the matrix abundance. Because the relative trend of the elastic properties presented in Figures 9a-c are similar, we focus on V_p in the following discussion.

From the seismological aspect, the wave velocity varies depending on where the wave travels within a heterogeneous medium (e.g., H. Sato et al., 2012). CM, CO, and CV chondrites contain inclusions such as chondrules and CAIs — possibly showing more inhomogeneous structures. Therefore there may be a correlation between the variation of elastic properties with the abundance of the matrix (or inclusions). The previous studies summarize the average matrix abundance of CI (95 vol%), CM (70 vol%), CO (30 vol%), CV (40 vol%), Tagish Lake and Tarda (80 vol%) (e.g., Scott & Krot, 2014; Blinova et al., 2014; Alexander, 2019; Chennaoui-Aoudjehane et al., 2021). Ryugu does not include CAIs or chondrule and almost all area is regarded as matrix (e.g., Yada et al., 2022; T. Nakamura et al., 2022).

Figure 10a shows that the variation of V_p becomes smaller with the matrix abundance as a general trend. However, the trend does not simply explain the variation of V_p between CM, CV, and CO chondrites (Figure 10a), where CV chondrites show a larger variation than CO. We found that the variation of V_p also relates to the mean chondrule size, where CV chondrites with a larger mean chondrule size show the larger V_p variation (Figure 10b). This trend is consistent with the idea that the seismic wave velocity varies depending on the path under inhomogeneous media (e.g., H. Sato et al., 2012), and the dynamic range of variation becomes larger when the contrast of elastic properties between the inclusions and matrix becomes stronger.

The cause for the variation of relative abundance and mean size of chondrules among different groups of chondrites is a long-standing problem in the planetary formation model (Jacquet, 2014; Simon et al., 2018). Although previous works were limited to chemical and mineralogical discussion, this study made it possible to discuss the problem from a novel point of view. More systematical measurements of the elastic property of chondrites and joint interpretation with other measurements would enable us to elucidate which sides of chondrule characteristics affect the elastic property and how the differences among carbonaceous chondrites stemmed from.

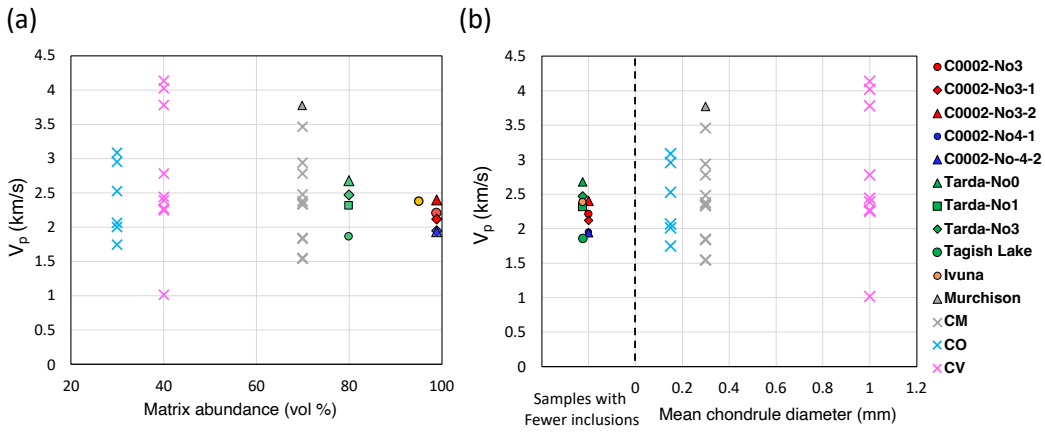

Figure 10. (a) Matrix abundance vs. P-wave velocity. The filled symbols represent our measurements and the colored crosses show the data from the previous measurements of CM, CO, and CV chondrites (Jones, 2009; Ibrahim, 2012; Cotto-Figueroa et al., 2016). The matrix abundances were referenced from Alexander (2019), Blinova et al. (2014), and Scott and Krot (2014) (See the text for the details). (b) Mean chondrule diameter vs. P-wave velocity. The mean chondrule diameters were from Scott and Krot (2014).

4 Concluding Remarks

We measured the seismic wave velocities of Ryugu samples and obtained the P- and S-wave velocities of about 2.1 km/s and 1.2 km/s, respectively. Combining those velocities with the bulk density gives Young's modulus of 6.0 – 8.0 GPa for the Ryugu samples. These elastic properties are similar to those of Tagish Lake (C2).

Combined with previous results (e.g., Yada et al., 2022; T. Nakamura et al., 2022; Yokoyama et al., 2022), we can characterize that the Ryugu samples are chemically CI-like but physically Tagish Lake-like. Both CI and Tagish Lake experienced aqueous alteration and do not hold inclusions such as CAIs and chondrules, and these might have undergone similar evolution processes. Thus, our results anyhow support the previous interpretation that Ryugu's parent body had formed in the outer solar system. By studying the differences in chemical and physical characteristics between these three samples, it would be possible to better constrain how differently each parent body formed and evolved. This should lead to a finer illustration of the early evolution of the solar system.

We obtained the Ryugu's quality factor Q of 10 – 20 which is similar to those of the Apollo returned lunar rocks. However, the Q in this study is the lower limit because the measurements were done at 1 atm and room temperature, and needs to be refined in future work.

This study provided the elastic properties of the returned asteroid sample for the first time and will be a milestone for a better understanding of the elastic behavior on asteroids such as resurfacing effect with seismic shaking and for better modeling of the formation and evolution processes of Ryugu. The next big step would be to consider how we can extrapolate the particle-scale properties to the regional and/or global scale. In future work, we plan to estimate the bulk elastic behavior by combining our measurement results with numerical simulations and other remote sensing data.

5 Data and Resources

The seismic signal data of the respective measurements and the X-ray CT image data of C0002-No3 and C0002-No4 are available at Onodera (2023).

Acknowledgments

The Hayabusa2 mission has been led by JAXA, in collaboration with DLR (German Space Center) and CNES (French Space Center), and was also supported by NASA, the ASA (Australian Space Agency) and other universities and institutes. We thank all of the members of the Hayabusa2 project team for their technical and scientific contributions to the successful return of the asteroid samples to Earth. We acknowledge SPring-8 and Brucker Japan for kindly sharing the X-ray CT image data for analysis. We are grateful to Prof. Akiko Nakamura and Dr. Yusuke Nakauchi for providing us with the Tagish Lake and Murchison meteorites, respectively. We also thank Dr. Akira Yoneda for providing us with transducers and an amplifier. This study was partly supported by the Hypervelocity Impact Facility of the Institute of Space and Astronautical Science, Japan Aerospace Exploration Agency.

References

Aki, K., & Richards, P. G. (1980). *Quantitative seismology, theory and methods* (Vol. 1). Freeman.

Alexander, C. M. O. (2019). Quantitative models for the elemental and isotopic fractionations in chondrites: The carbonaceous chondrites. *Geochimica et Cosmochimica Acta*, *254*, 277-309. doi: https://doi.org/10.1016/j.gca.2019.02.008

Arakawa, M., Saiki, T., Wada, K., Ogawa, K., Kadono, T., Shirai, K., ... Miura, A. (2020). An artificial impact on the asteroid (162173) ryugu formed a crater in the gravity-dominated regime. *Science*, *368*(6486), 67-71. doi: 10.1126/science.aaz1701

Birch, F. (1960). The velocity of compressional waves in rocks to 10 kilobars: 1. *Journal of Geophysical Research (1896-1977)*, *65*(4), 1083-1102. doi: https://doi.org/10.1029/JZ065i004p01083

Blanchette-Guertin, J.-F., Johnson, C. L., & Lawrence, J. F. (2012). Investigation of scattering in lunar seismic coda. *Journal of Geophysical Research: Planets*, *117*(E6). doi: https://doi.org/10.1029/2011JE004042

Blinova, A., Zega, T., Herd, C., & Stroud, R. (2014, April). Testing variations within the tagish lake meteorite-i: Mineralogy and petrology of pristine samples. *Meteoritics and Planetary Science*, *49*(4), 473–502. doi: 10.1111/maps.12271

Chennaoui-Aoudjehane, H., Agee, C., Ziegler, K., Garvie, L., Irving, A., Sheikh, D., ... Trif, L. (2021). Tarda an unusual carbonaceous meteorite fall from morocco. In *Proceedings of 84th annual meeting of the meteoritical society* (p. 6303).

Cotto-Figueroa, D., Asphaug, E., Garvie, L. A., Rai, A., Johnston, J., Borkowski, L., ... Morris, M. A. (2016). Scale-dependent measurements of meteorite strength: Implications for asteroid fragmentation. *Icarus*, *277*, 73-77. doi: https://doi.org/10.1016/j.icarus.2016.05.003

Grott, M., Knollenberg, J., M. Hamm, K. O., Jaumann, R., Otto, K. A., Delbo, M., ... Moussi-Soffys, A. (2019). Low thermal conductivity boulder with high porosity identified on c-type asteroid (162173) ryugu. *Nature Astronomy*, *3*, 971–976.

Honda, R., Arakawa, M., Shimaki, Y., Shirai, K., Yokota, Y., Kadono, T., ... ichi Iijima, Y. (2021). Resurfacing processes on asteroid (162173) ryugu caused by an artificial impact of hayabusa2's small carry-on impactor. *Icarus*, *366*, 114530. doi: https://doi.org/10.1016/j.icarus.2021.114530

Ibrahim, E.-M. (2012). *The elastic properties of carbonaceous chondrites.* PRISM. doi: 10.11575/PRISM/10182

Ito, M., Tomioka, N., Uesugi, M., Yamaguchi, A., Shirai, N., Ohigashi, T., ... Tsuda, Y. (2022). A pristine record of outer solar system materials from asteroid ryugu's returned sample. *Nature Astronomy*, *6*, 1163-1171. doi: 10.1038/s41550-022-01745-5

Jacquet, E. (2014). The quasi-universality of chondrule size as a constraint for chondrule formation models. *Icarus*, *232*, 176-186. doi: https://doi.org/10.1016/j.icarus.2014.01.012

Jones, S. F. (2009). *Elastic wave velocity, porosity, and pore geometry of ordinary chondrites and artificially shocked samples.* PRISM. doi: 10.11575/PRISM/10182

Kanamori, H., Mizutani, H., & Hamano, Y. (1971). Elastic wave velocities of apollo 12 rocks at high pressures. In *Proceedings of the second lunar science conference* (Vol. 3, p. 2323-2326).

Kanamori, H., Nur, A., Chung, D., Wones, D., & Simmons, G. (1970). Elastic wave velocities of lunar samples at high pressures and their geophysical implications. *Science*, *167*(3918), 726-728. doi: 10.1126/science.167.3918.726

Morota, T., Sugita, S., Cho, Y., Kanamaru, M., Tatsumi, E., Sakatani, N., ... Tsuda, Y. (2020). Sample collection from asteroid (162173) ryugu by hayabusa2: Implications for surface evolution. *Science*, *368*(6491), 654-659. doi: 10.1126/science.aaz6306

Nakamura, T., Matsumoto, M., Amano, K., Enokido, Y., Zolensky, M. E., Mikouchi, T., ... Tsuda, Y. (2022). Formation and evolution of carbonaceous asteroid ryugu: Direct evidence from returned samples. *Science*, *0*(0), eabn8671. doi: 10.1126/science.abn8671

Nakamura, Y., & Koyama, J. (1982). Seismic q of the lunar upper mantle. *Journal of Geophysical Research: Solid Earth*, *87*(B6), 4855-4861.

Nakashima, K., Kawasaki, N., Sakamoto, N., Yurimoto, T. H. i. a. c. t., H., & initial analysis core, T. H. (2022). In-situ oxygen and manganese-chromium isotpe studies of ryugu: Implications to temperature and timing of aqueous activity. In *Proceedings of 53rd lunar and planetary science conference* (p. 1689).

Nishiyama, G., Kawamura, T., Namiki, N., Fernando, B., Leng, K., Onodera, K., ... Iijima, Y. (2021). Simulation of seismic wave propagation on asteroid ryugu induced by the impact experiment of the hayabusa2 mission: Limited mass transport by low yield strength of porous regolith. *Journal of Geophysical Research: Planets*, *126*(2), e2020JE006594. (e2020JE006594 2020JE006594) doi: https://doi.org/10.1029/2020JE006594

Onodera, K. (2023). *Seismic signal data and X-ray CT image data of Hayabusa2 returned samples.* doi: 10.5281/zenodo.7860955

Onodera, K., Kawamura, T., Tanaka, S., Ishihara, Y., & Maeda, T. (2022). Quantitative evaluation of the lunar seismic scattering and comparison between the earth, mars, and the moon. *Journal of Geophysical Research: Planets*, *127*(12), e2022JE007558. doi: https://doi.org/10.1029/2022JE007558

Onodera, K., Maeda, T., Nishida, K., Kawamura, T., Margerin, L., Menina, S., ... Banerdt, W. B. (2023). Seismic scattering and absorption properties of mars estimated through coda analysis on a long-period surface wave of s1222a marsquake. *Geophysical Research Letters*, *50*, e2022GL102716. doi: https://doi.org/10.1029/2022GL102716

Ostrowski, D., & Bryson, K. (2019). The physical properties of meteorites. *Planetary and Space Science*, *165*, 148-178. doi: https://doi.org/10.1016/j.pss.2018.11.003

Richardson, J. E., Melosh, H. J., & Greenberg, R. (2004). Impact-induced seismic activity on asteroid 433 eros: A surface modification process. *Science*,

306(5701), 1526-1529. doi: 10.1126/science.1104731

Saiki, T., Sawada, H., Okamoto, C., Yano, H., Takagi, Y., Akahoshi, Y., & Yoshikawa, M. (2013). Small carry-on impactor of hayabusa2 mission. *Acta Astronautica*, *84*, 227-236. doi: https://doi.org/10.1016/j.actaastro.2012.11.010

Sato, H., Fehler, M. C., & Maeda, T. (2012). *Seismic wave propagation and scattering in the heterogeneous earth: Second edition.* Springer Berlin, Heidelberg. doi: 10.1007/978-3-642-23029-5

Sato, M., Kimura, Y., Tanaka, S., Hatakeyama, T., Sugita, S., Nakamuna, T., ... Tsuda, Y. (2022). Rock magnetic characterization of returned samples from asteroid (162173) ryugu: Implications for paleomagnetic interpretation and paleointensity estimation. *Journal of Geophysical Research: Planets*, *127*(11), e2022JE007405. (e2022JE007405 2022JE007405)

Scott, E., & Krot, A. (2014). 1.2 - chondrites and their components. In H. D. Holland & K. K. Turekian (Eds.), *Treatise on geochemistry (second edition)* (Second Edition ed., p. 65-137). Oxford: Elsevier. doi: https://doi.org/10.1016/B978-0-08-095975-7.00104-2

Simon, J., Cuzzi, J., McCain, K., Cato, M., Christoffersen, P., Fisher, K., ... Scargle, J. (2018). Particle size distributions in chondritic meteorites: Evidence for pre-planetesimal histories. *Earth and Planetary Science Letters*, *494*, 69-82. doi: https://doi.org/10.1016/j.epsl.2018.04.021

Sugita, S., Honda, R., Morota, T., Kameda, S., Sawada, H., Tatsumi, E., ... Tsuda, Y. (2019). The geomorphology, color, and thermal properties of ryugu: Implications for parent-body processes. *Science*, *364*(6437), eaaw0422. doi: 10.1126/science.aaw0422

Tachibana, S., Sawada, H., Okazaki, R., Takano, Y., Sakamoto, K., Miura, Y. N., ... Tsuda, Y. (2022). Pebbles and sand on asteroid (162173) ryugu: In situ observation and particles returned to earth. *Science*, *375*(6584), 1011-1016. doi: 10.1126/science.abj8624

Takaki, N., Cho, Y., Morota, T., Tatsumi, E., Honda, R., Kameda, S., ... Sugita, S. (2022). Resurfacing processes constrained by crater distribution on ryugu. *Icarus*, *377*, 114911. doi: https://doi.org/10.1016/j.icarus.2022.114911

Tittman, B. R. (1977). Lunar rock q in 3000-5000 range achieved in laboratory. *Philosophical Transactions of the Royal Society of London. Series A, Mathematical and Physical Sciences*, *285*(1327), 475-479. doi: 10.1098/rsta.1977.0090

Tittman, B. R., Abdel-Gawad, M., & Houseley, R. M. (1972). Elastic velocity and q factor measurements on apollo 12, 14, and 15 rocks. In *Proceedings of the third lunar science conference* (Vol. 3, p. 2565-2575).

Tittman, B. R., Ahlberg, L., & Curnow, J. (1976). Internal friction and velocity measurements. In *Proceedings of lunar and planetary science conference* (Vol. 7, p. 3123-3132).

Tittman, B. R., Curnow, J., & Housley, R. (1975). Internal friction quality factor q greater than or equal to 3100 achieved in lunar rock 70215,85. In *Proceedings of lunar and planetary science conference* (Vol. 6, p. 3217-3226).

Wang, H., Todd, T., Weidner, D., & Simmons, G. (1971). Elastic properties of apollo 12 rocks. In *Proceedings of the second lunar science conference* (Vol. 3, p. 2327-2336).

Yada, T., Abe, M., Tatsuaki Okada, A. N., Yogata, K., Miyazaki, A., Hatakeda, K., ... Tsuda, Y. (2022). Preliminary analysis of the hayabusa2 samples returned from c-type asteroid ryugu. *Nature Astronomy*, *6*, 214-220. doi: 10.1038/s41550-021-01550-6

Yokoyama, T., Nagashima, K., Nakai, I., Young, E. D., Abe, Y., Aléon, J., ... Yurimoto, H. (2022). Samples returned from the asteroid ryugu are similar to ivuna-type carbonaceous meteorites. *Science*, *0*(0), eabn7850. doi:

10.1126/science.abn7850

Zolensky, M. E., Nakamura, K., Gounelle, M., Mikouchi, T., Kasama, T., Tachikawa, O., & Tonui, E. (2002). Mineralogy of tagish lake: An ungrouped type 2 carbonaceous chondrite. *Meteoritics & Planetary Science*, *37*(5), 737-761. doi: https://doi.org/10.1111/j.1945-5100.2002.tb00852.x

Figure1.

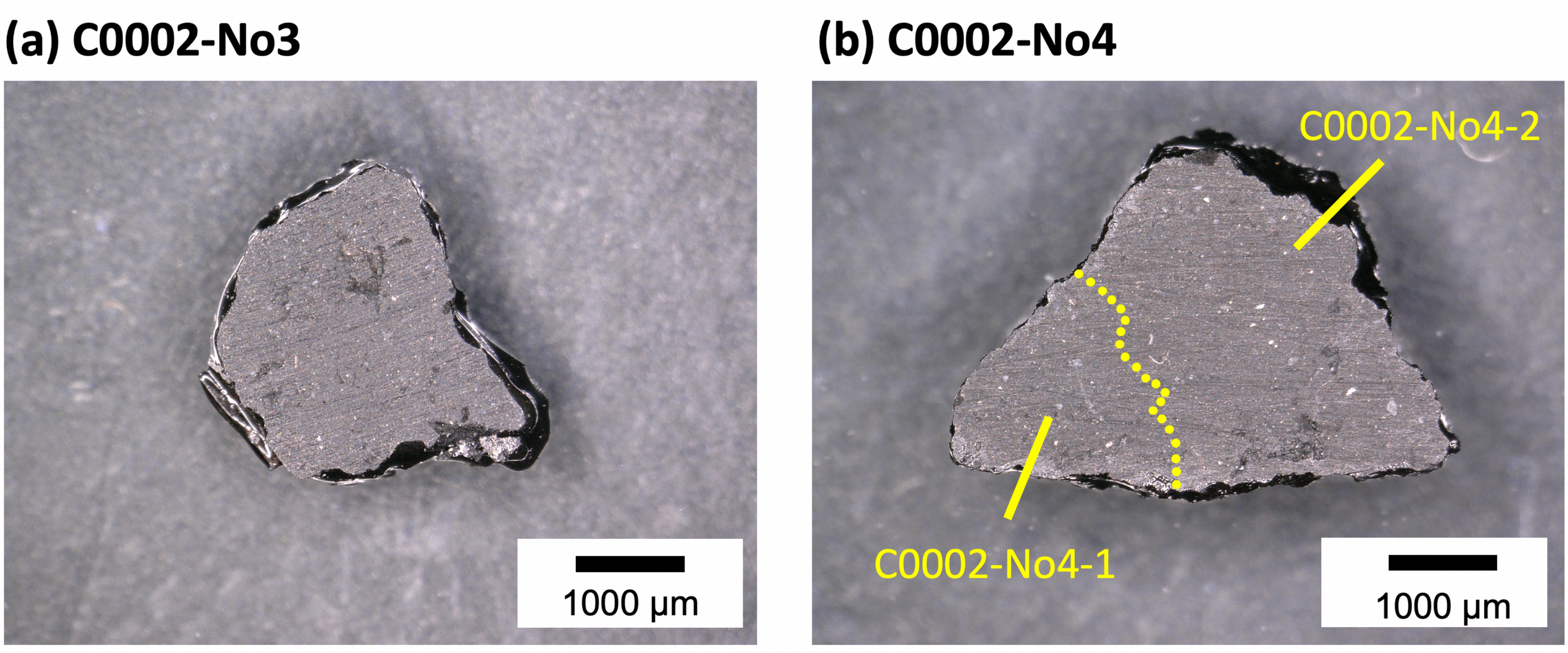
(a) C0002-No3
1000 μm
(b) C0002-No4
C0002-No4-2
C0002-No4-1
1000 μm

Figure2.

(a)

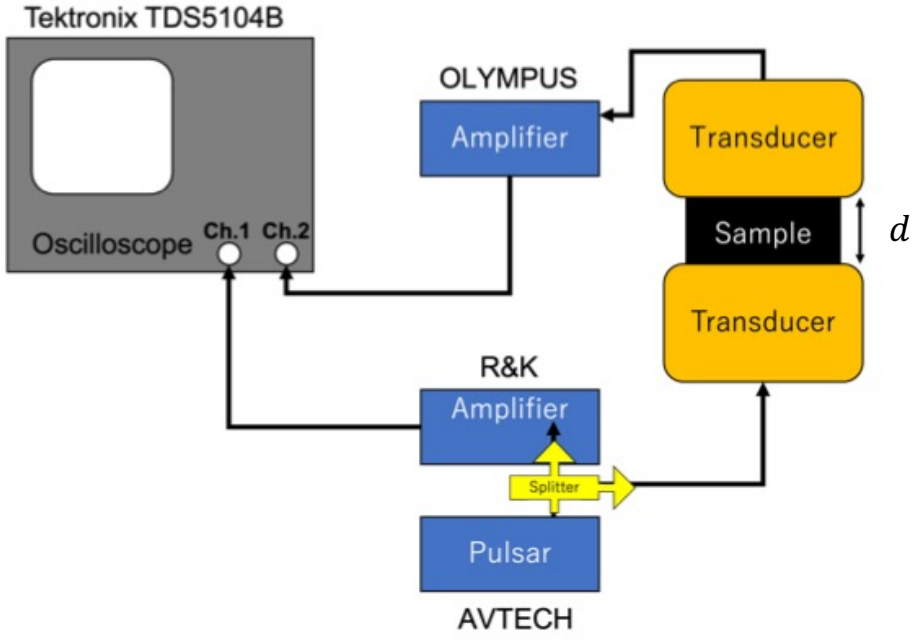

(b)

Pulsar	AVTECH, AVL-2-C-M-P
Amplifier	R&K, A-308 (Receiver-side)
	OLYMPUS, 5073PR (Transmitter-side)
Oscilloscope	Tektronix, TDS5104B
Splitter	Mini-Circuits, ZFSC-2-4
Transducers	P-wave: OLYMPUS, V202, V116 S-wave: OLYMPUS, V222-BC-RM, V222-BC

(c)

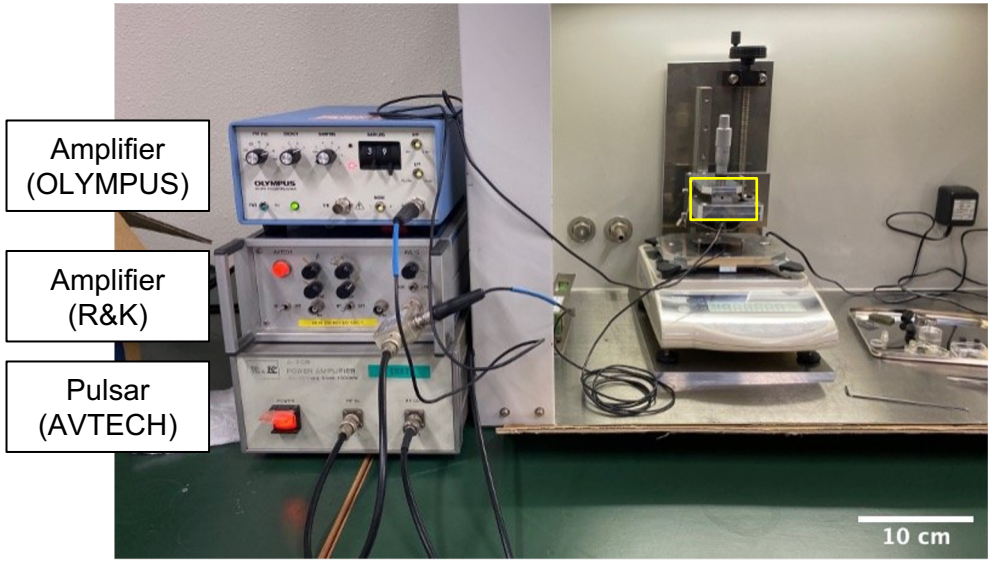

(d)

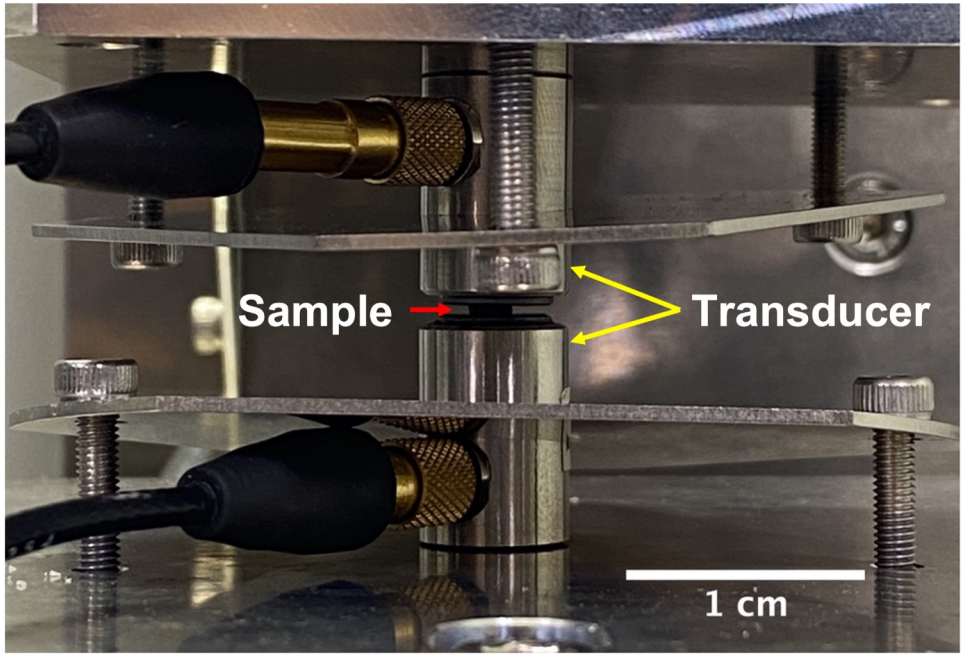

Figure3.

(a)

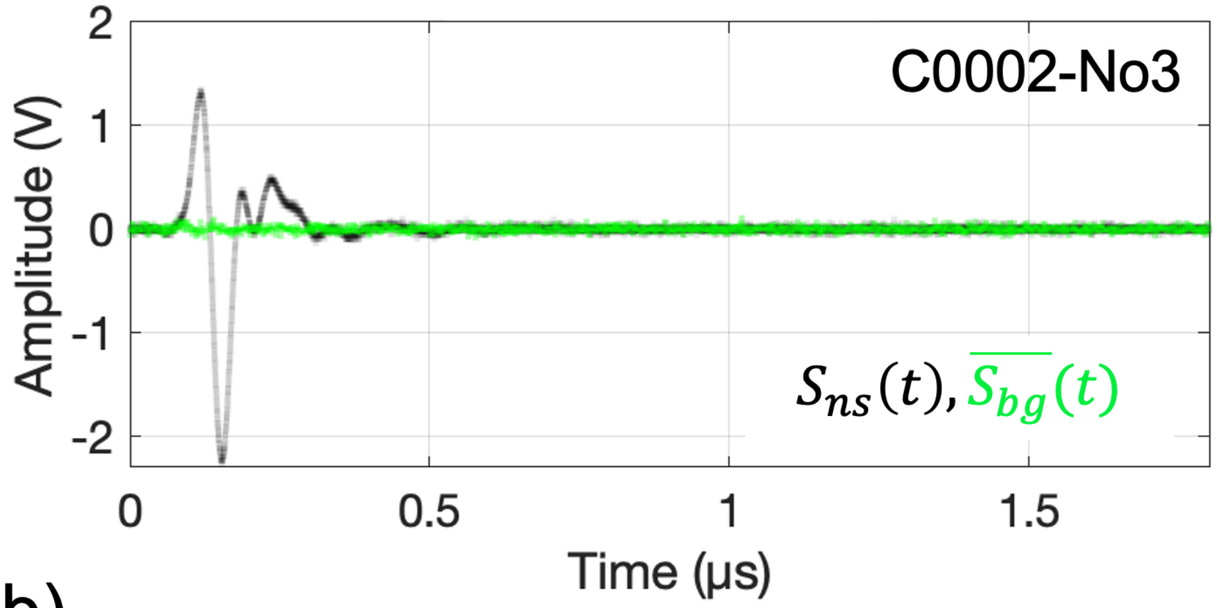
C0002-No3
$S_{ns}(t), \overline{S_{bg}}(t)$
Amplitude (V)
Time (μs)

(b)

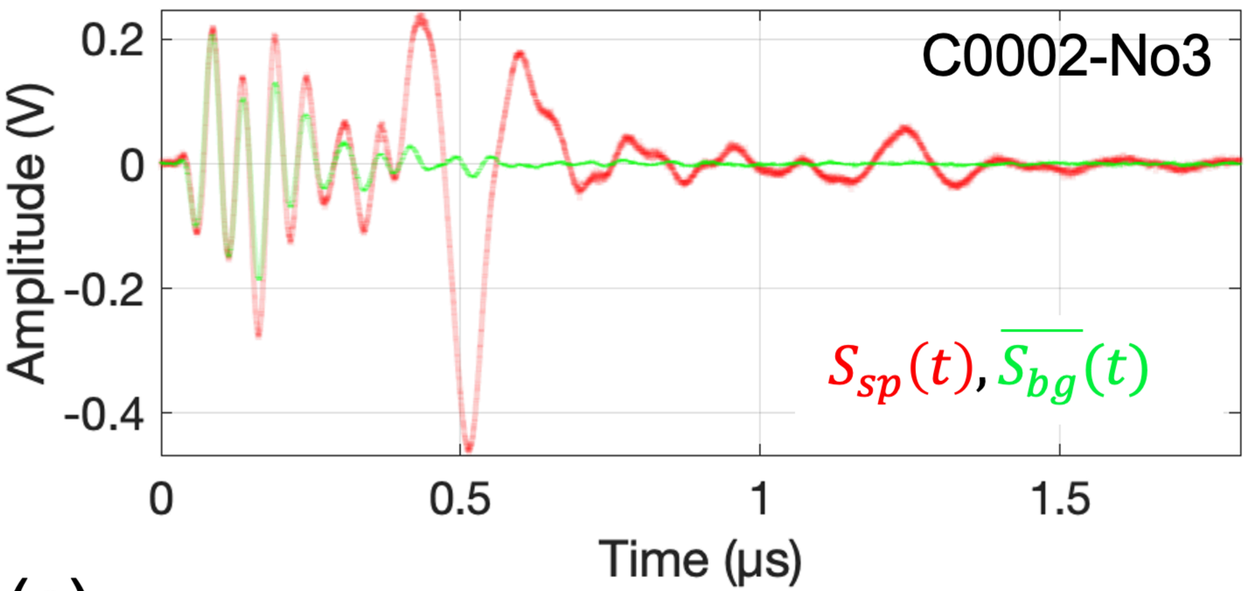
C0002-No3
$S_{sp}(t), \overline{S_{bg}}(t)$
Amplitude (V)
Time (μs)

(c)

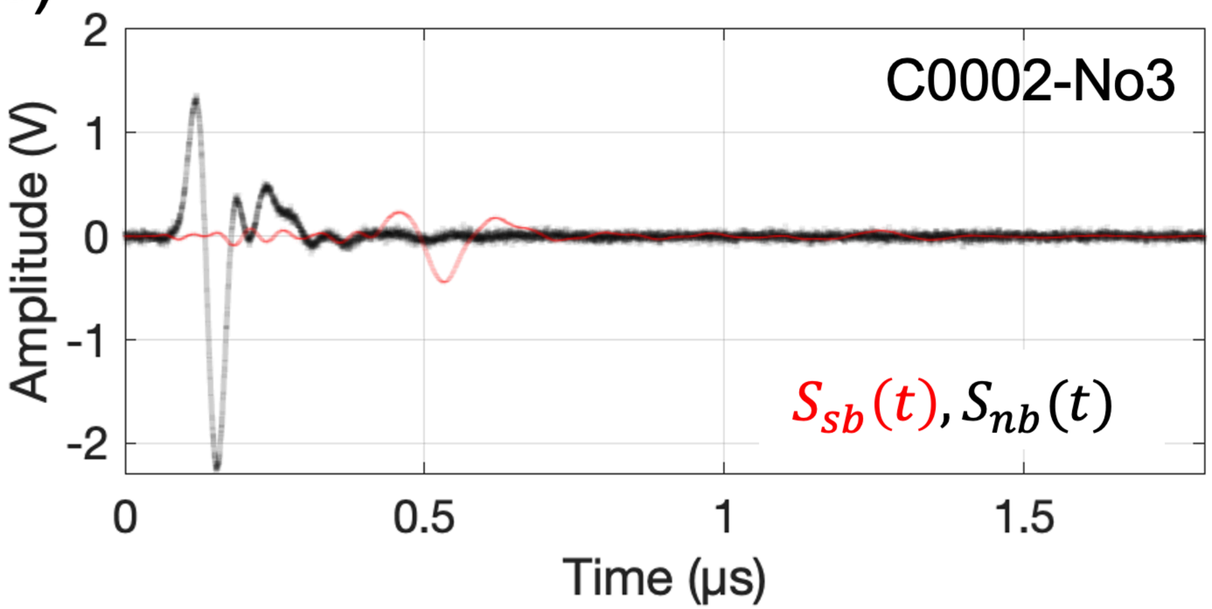
C0002-No3
$S_{sb}(t), S_{nb}(t)$
Amplitude (V)
Time (μs)

(d)

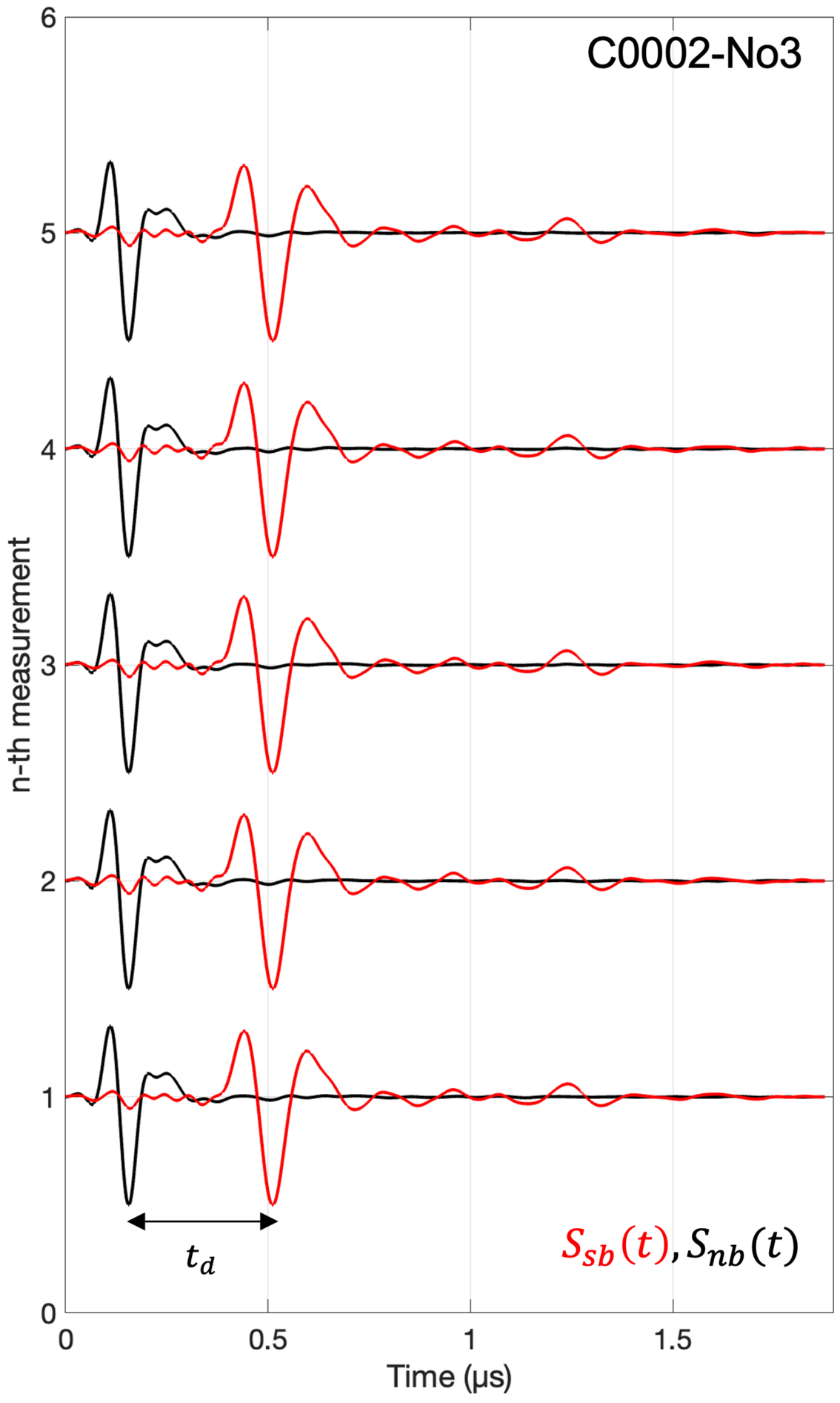
C0002-No3
$S_{sb}(t), S_{nb}(t)$
t_d
n-th measurement
Time (μs)

Figure4.

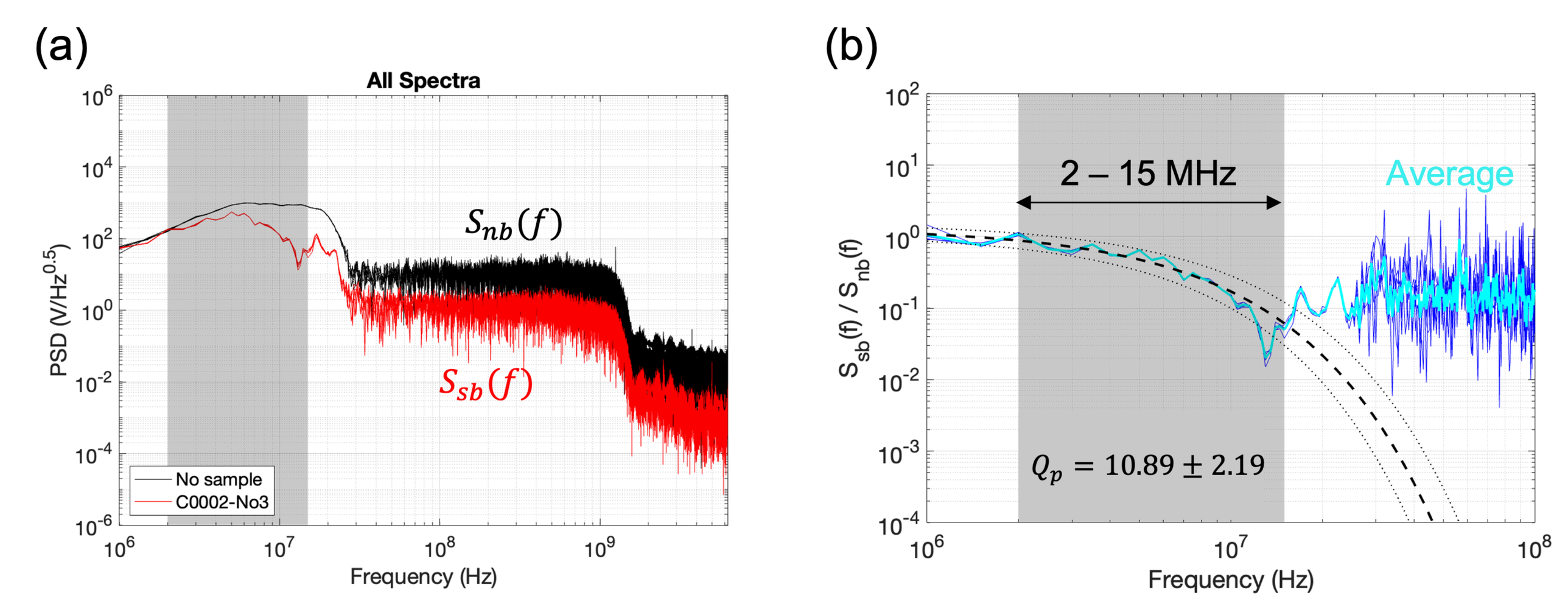
(a)
All Spectra
$S_{nb}(f)$
$S_{sb}(f)$
No sample
C0002-No3
PSD (V/Hz$^{0.5}$)
Frequency (Hz)
(b)
2 – 15 MHz
Average
$Q_p = 10.89 \pm 2.19$
$S_{sb}(f) / S_{nb}(f)$
Frequency (Hz)

Figure5.

(a) Before destruction

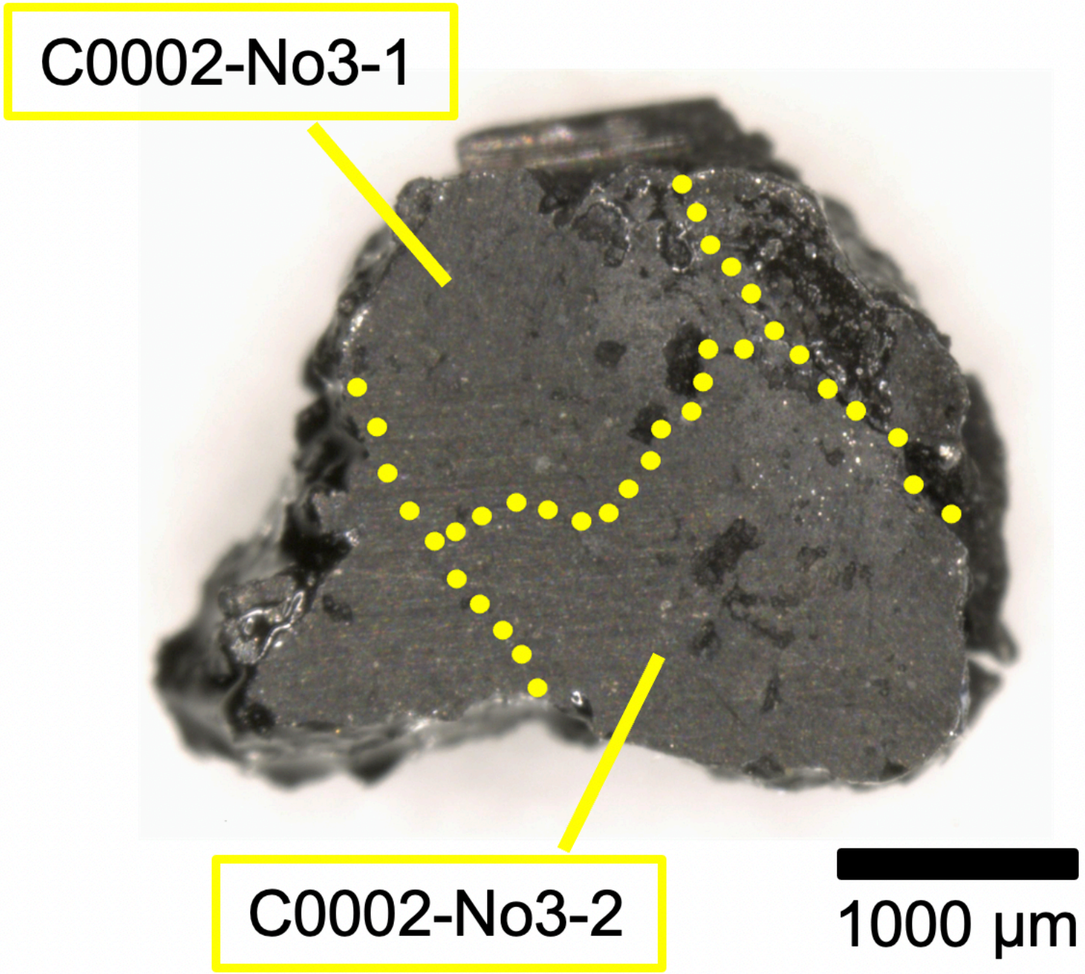

(b) After destruction

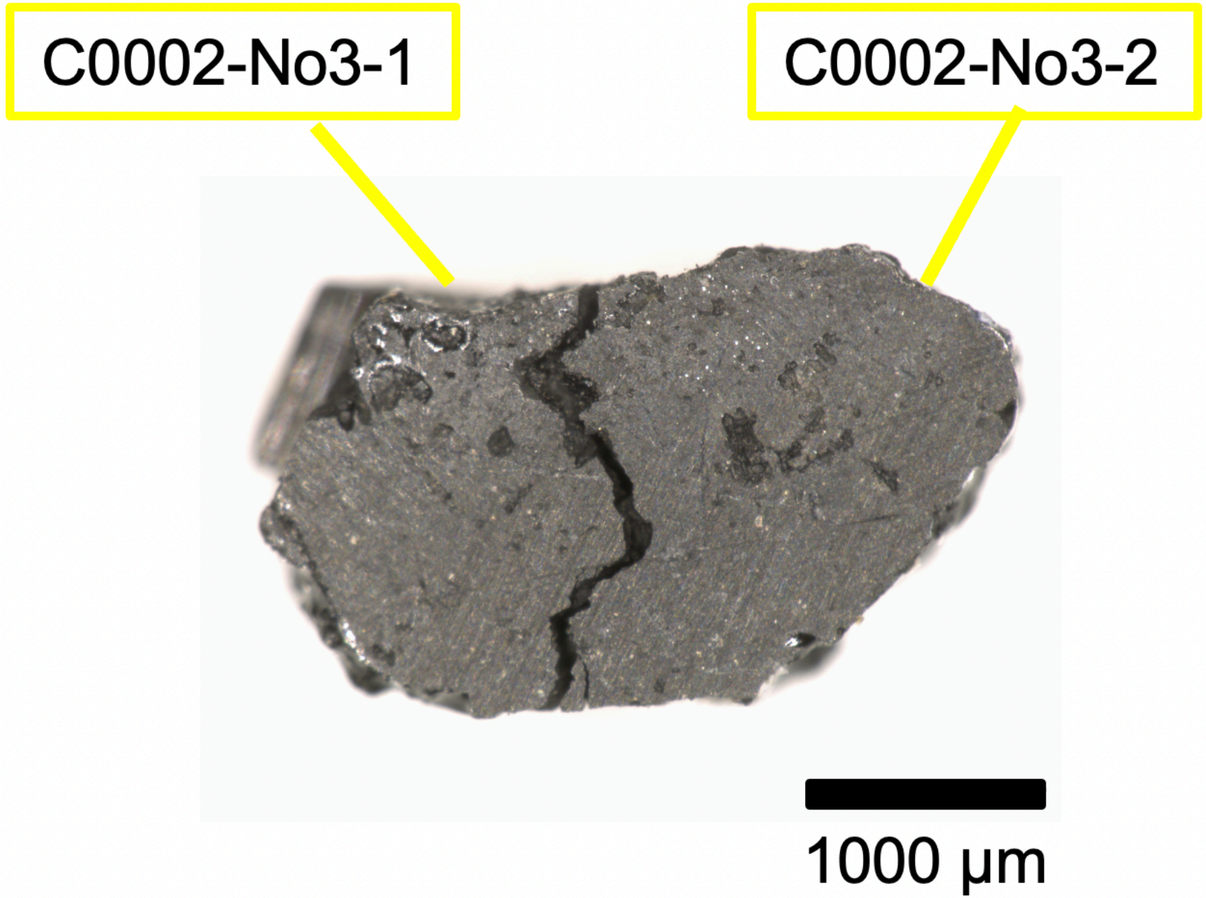

Figure6.

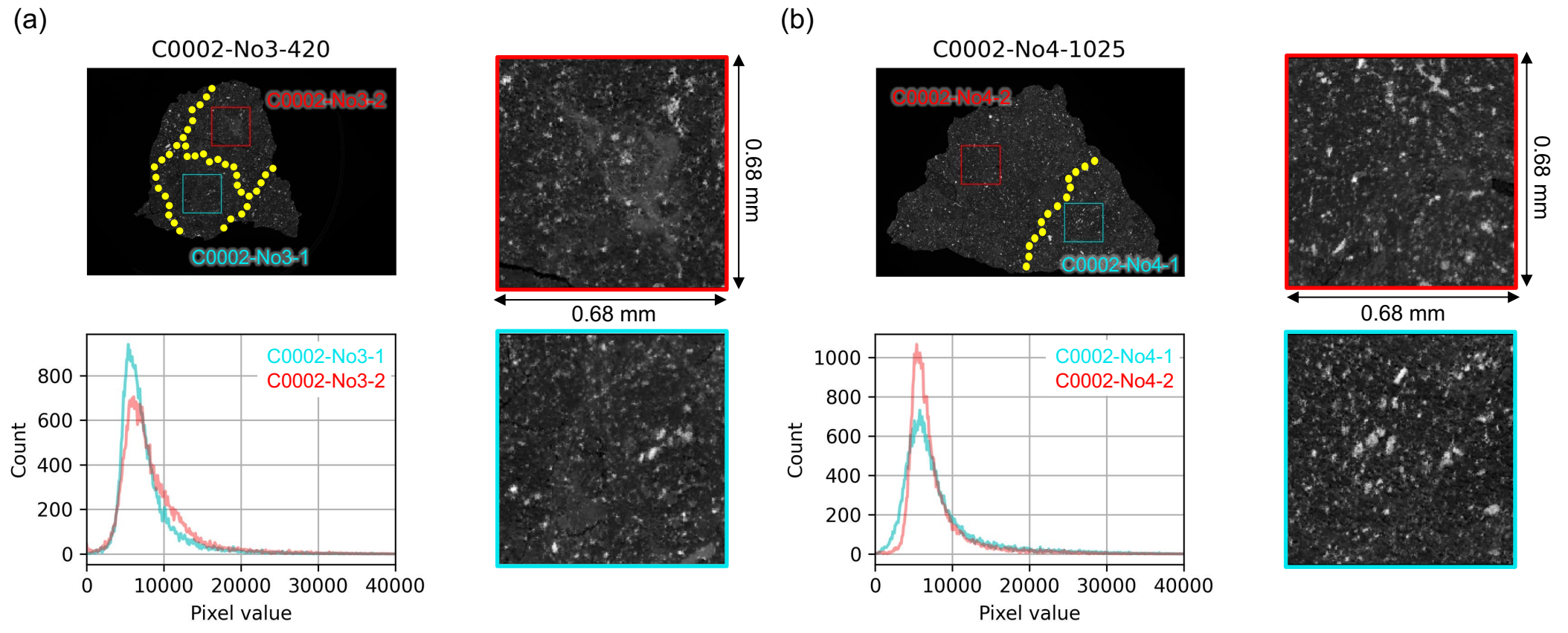
(a)
C0002-No3-420
C0002-No3-2
C0002-No3-1
0.68 mm
0.68 mm
C0002-No3-1
C0002-No3-2
Count
Pixel value
(b)
C0002-No4-1025
C0002-No4-2
C0002-No4-1
0.68 mm
0.68 mm
C0002-No4-1
C0002-No4-2
Count
Pixel value

Figure7.

C0002-No3-2 (Slice 420)

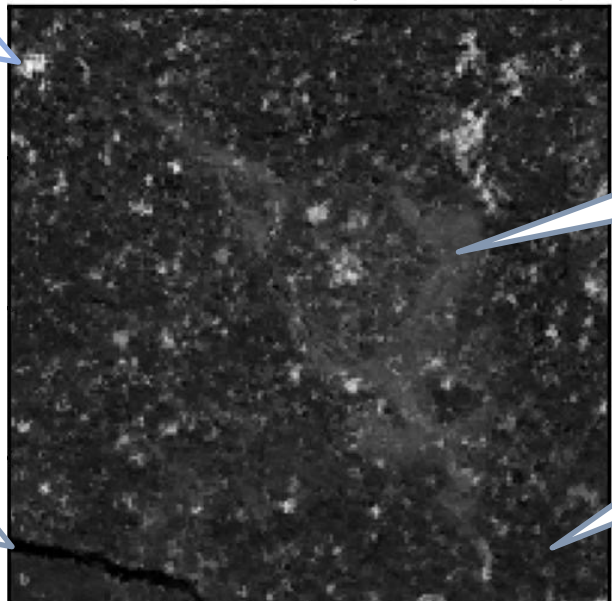

Figure8.

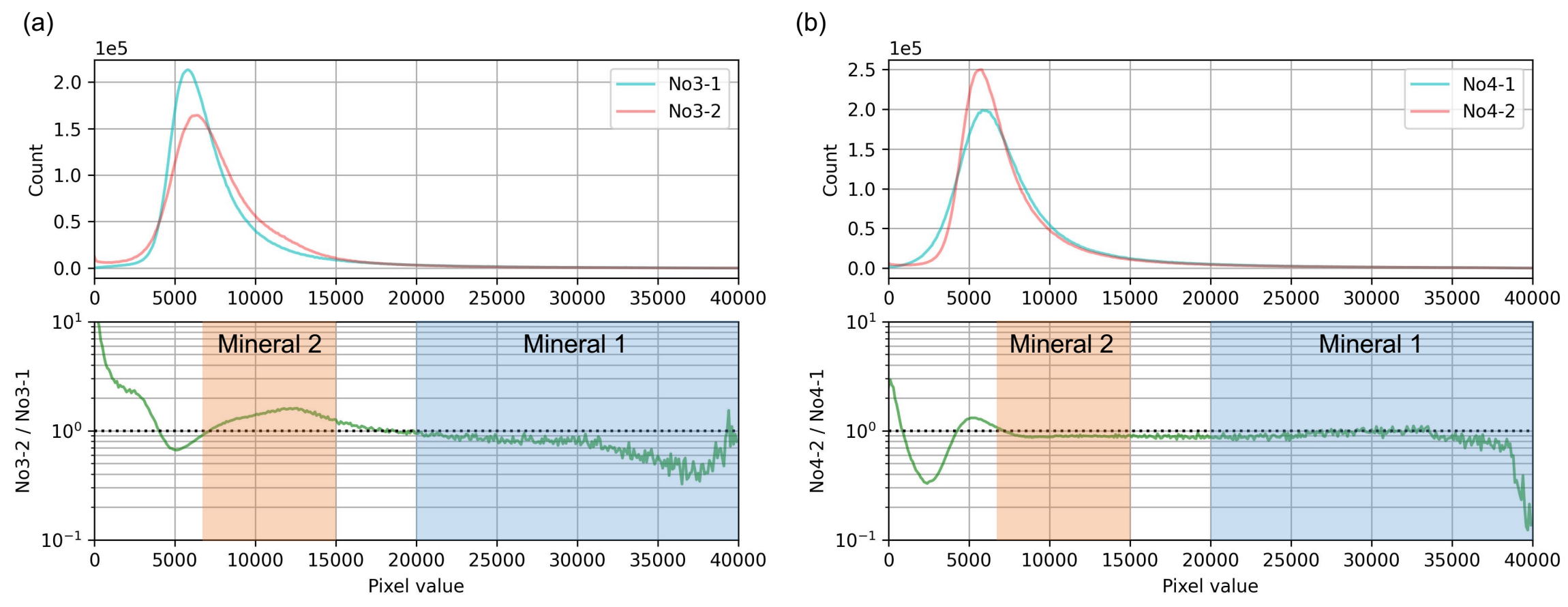
(a)
1e5
Count
No3-1
No3-2
Mineral 2
Mineral 1
No3-2 / No3-1
Pixel value
(b)
1e5
Count
No4-1
No4-2
Mineral 2
Mineral 1
No4-2 / No4-1
Pixel value

Figure9.

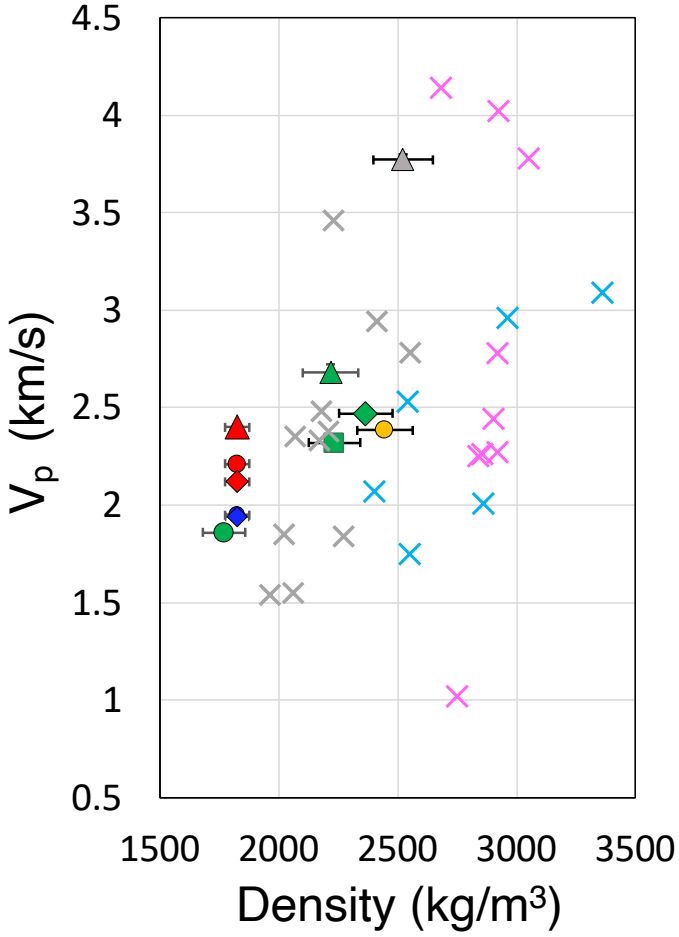
4.5
4
3.5
3
2.5
2
1.5
1
0.5
V_p (km/s)
1500
2000
2500
3000
3500
Density (kg/m^3)

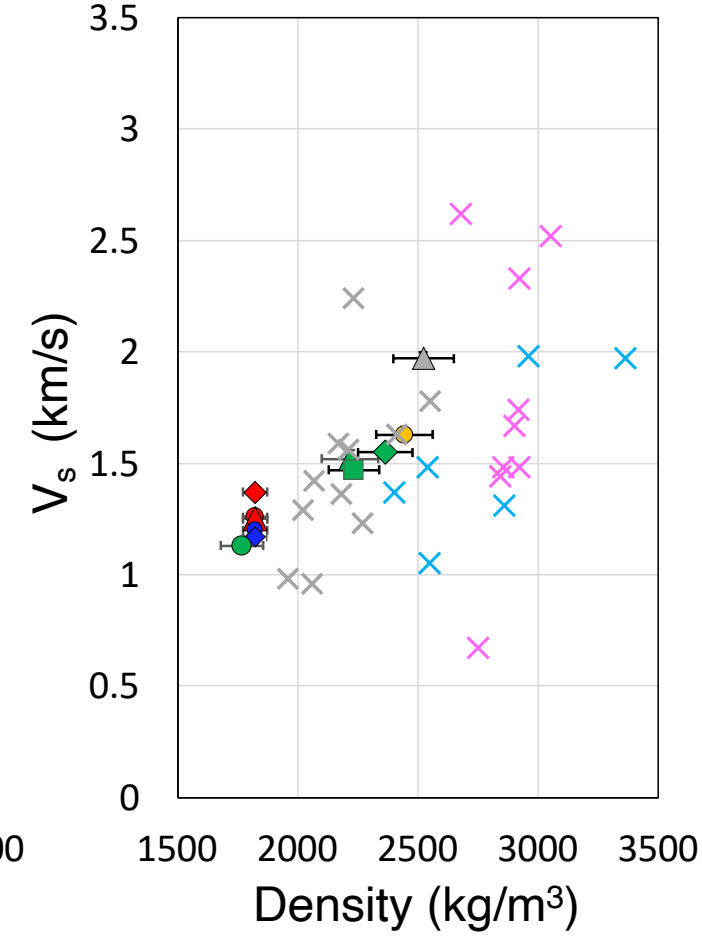
3.5
3
2.5
2
1.5
1
0.5
0
V_s (km/s)
1500
2000
2500
3000
3500
Density (kg/m^3)

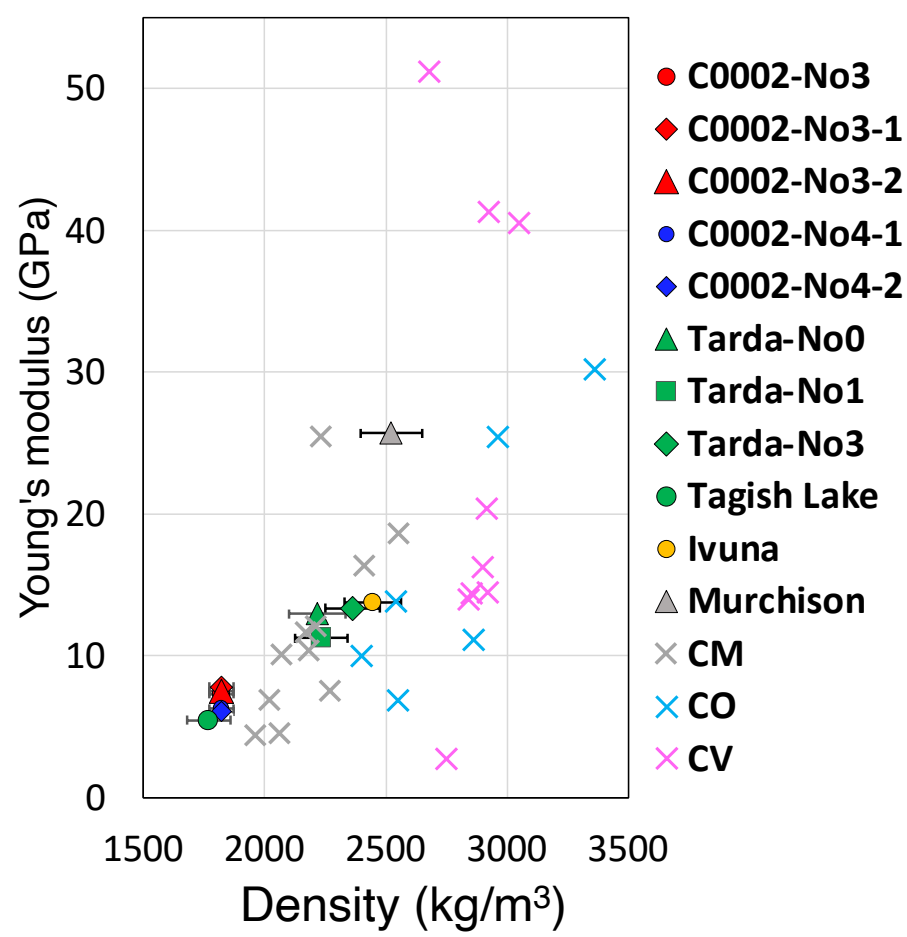
50
40
30
20
10
0
Young's modulus (GPa)
1500
2000
2500
3000
3500
Density (kg/m^3)
C0002-No3
C0002-No3-1
C0002-No3-2
C0002-No4-1
C0002-No4-2
Tarda-No0
Tarda-No1
Tarda-No3
Tagish Lake
Ivuna
Murchison
CM
CO
CV

Figure10.

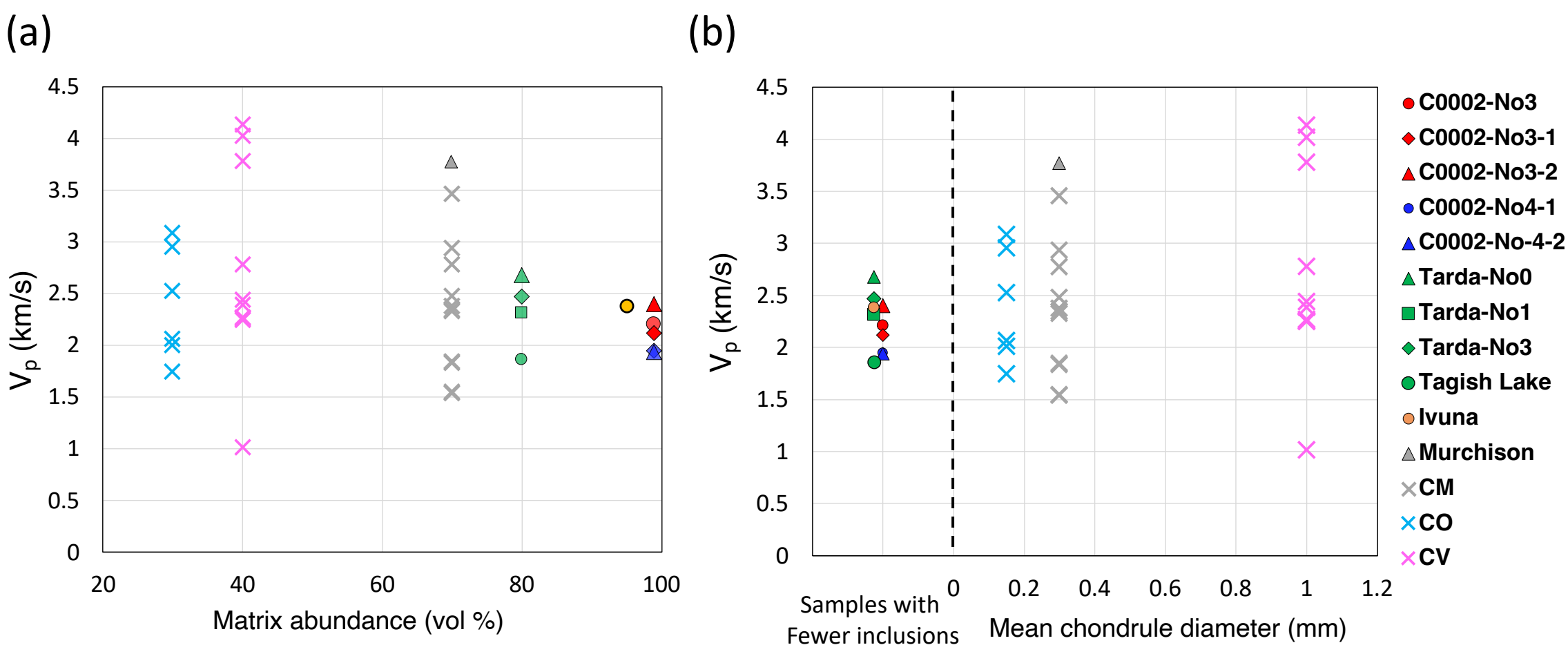
(a)
(b)
V_p (km/s)
Matrix abundance (vol %)
Samples with Fewer inclusions
Mean chondrule diameter (mm)
C0002-No3
C0002-No3-1
C0002-No3-2
C0002-No4-1
C0002-No-4-2
Tarda-No0
Tarda-No1
Tarda-No3
Tagish Lake
Ivuna
Murchison
CM
CO
CV